RSC Advances

REVIEW

View Article Online
View Journal | View Issue

Cite this: *RSC Adv.*, 2024, **14**, 26837

Research progress of functional MXene in inhibiting lithium/zinc metal battery dendrites

Haiyan Wang, *[ab] Mengxin Ning,[b] Min Sun,[b] Bin Li,[b] Yachuan Liang[ab] and Zijiong Li*[b]

The layered two-dimensional (2D) MXene has great promise for applications in supercapacitors, batteries, and electrocatalysis due to its large layer spacing, excellent electrical conductivity, good chemical stability, good hydrophilicity, and adjustable layer spacing. Since its discovery in 2011, MXene has been widely used to inhibit the growth of anode dendrites of lithium metal. In the past two years, researchers have used MXene and MXene based materials in the anodes of zinc metal batteries and zinc ion hybrid capacitors, respectively, and made a series of important progressive steps in the inhibition of zinc dendrite growth. In this review, we summarize the research progress of functional MXenes in inhibiting the growth of lithium and zinc metal anode dendrites, and provide a brief overview and outlook on the current challenges of MXene materials, which will help researchers to further understand the methods and their mechanisms, thus to develop novel electrochemical energy storage systems to meet the needs of rapidly developing electric vehicles and wearable/portable electronics.

Received 18th July 2024
Accepted 15th August 2024

DOI: 10.1039/d4ra05220j

rsc.li/rsc-advances

1. Introduction

Advanced energy storage technology is one of the intrinsic drivers of modern life.[1] Human survival and sustainable development are closely related to energy, and the extraction and utilization of other resources are also dependent on energy. Issues such as increasing population, global warming and environmental problems caused by massive burning of fossil fuels, increasing costs of fossil fuel extraction and distribution, and regional conflicts due to uneven distribution of limited fossil fuel reserves have made it imperative for modern societies to move away from their dependence on fossil fuels.[2–4] In view of the increasing problems such as climate deterioration and environmental pollution, it has become an inevitable trend to develop renewable and clean energy sources to gradually replace fossil energy sources. However, there are great differences in energy density and power density, lifetime, efficiency, and cost among multiple storage technologies, such as wind and/or solar, renewable energy sources that are highly influenced by time and geography and exist intermittently. This has prompted the search for safe, economical, sustainable and efficient electrochemical energy storage and conversion technologies.[5]

Batteries, as devices capable of converting energy between electrical and chemical energy, are some of the best means of achieving centralized storage of electrical energy and they play an important role in the utilization and development of new energy sources.[2,6,7] After the invention of the first voltaic battery by Count Volta, researchers have developed several batteries for commercialization, including lead-acid, nickel–cadmium, nickel–metal hydride, and lithium-ion secondary batteries,[8,9] and these electrical energy storage systems, especially lithium-ion secondary batteries, have revolutionized communication and transportation in modern life, enabling portable camcorders, cell phones, laptops and, more recently, electric cars.[10] However, over the past 150 years, the actual energy density of commercial batteries has increased only six-fold from the first generation of lead-acid batteries (~40 W h kg^{-1}) to the current lithium-ion batteries (~240 W h kg^{-1} and ~40 640 W h L^{-1}).[6,9] This implies that the actual energy density of current commercial batteries has increased slowly, despite the phenomenal growth in lithium-ion battery sales worldwide. This is because lithium-ion batteries have almost reached the theoretical value of positive/negative electrodes, especially graphite negative electrodes (the theoretical capacity is only 372 mA h g^{-1}). In the face of the high demand for high energy density in emerging sophisticated electronic devices, it is urgent to develop higher energy density electrode materials.

However, just meeting the demand for high energy density is far from meeting the actual development needs of batteries. A series of accidents caused by potential safety problems of batteries, such as the Tesla electric car fire and Samsung cell phone explosion, have also seriously hindered the commercial application and promotion of batteries. Therefore, in the face of the current energy crisis and the actual market demand, the safety and cost of batteries also need to be considered comprehensively, and the development of high-performance

[a]*Academy for Quantum Science and Technology, Zhengzhou University of Light Industry, Zhengzhou 450002, PR China. E-mail: haiyan.wang@163.com*
[b]*School of Electronics and Information, Zhengzhou University of Light Industry, Zhengzhou 450002, PR China. E-mail: zijongli@zzuli.edu.cn*

batteries with higher energy density, higher safety, lower cost, and longer life has been the goal pursued by the battery industry.[4,11,12]

As one of the components of a battery, the structure and composition of electrode materials have a large impact on the electrochemical performance of the batteries.[8] The development of electrode materials with high energy density is essential to enhance the energy density of batteries. Numerous studies have shown that high energy density electrode materials (*e.g.*, silicon, antimony, red phosphorus, and tin materials), usually suffer from common problems in general.[13,14]

(1) The large volume changes bring the changes in the stress within the material in cycling process generates. When the stress changes exceed the limits of the material structure, the electrode material will break up and pulverize, causing irreversible structural damage or even detachment from the collector fluid. For the negative electrode, volume expansion also destroys the structure of the solid electrolyte interface (SEI) film, resulting in continuous lithium depletion and increased impedance, leading to severe deterioration in battery performance.[9]

(2) Most electrode materials have average electrical conductivity and slow ion/electron transport.

(3) For high energy density lithium/zinc metal anodes, their main scientific problem is that uncontrollable dendrite growth may puncture the diaphragm, leading to short circuiting of the battery and causing safety problems. In the face of the current urgent need for energy, it is essential to use of new materials, methods or mechanisms to solve these problems for the development of next-generation high-energy-density battery systems.[15–21]

The layered 2D MXene material has great promise for applications in supercapacitors, batteries, and electrocatalysis due to its large layer spacing, excellent electrical conductivity, good chemical stability, good hydrophilicity, and adjustable layer spacing.[22,23] MXenes are 2D layered materials derived from transition metal carbon/nitrogen/carbon nitrides (*e.g.*, Ti_3C_2).[24] In recent years, MXene materials have made great progress in the inhibition of metal dendrites, and a review on MXene inhibition of metal dendrites has not been reported. In this review, the methods and mechanisms of MXene materials to inhibit the growth of dendrites of lithium and zinc metals are introduced, focusing on the inhibition of zinc dendrites by MXene materials.

2. MXenes

MXenes are mainly compounds based on single metal carbides, such as Ti_3C_2, Ti_4C_3, V_2C, V_4C_3, *etc.* MXenes with binary metals as M-layers (Mo_2TiC_2 and $Mo_2Ti_2C_3$) have also been reported one after another, and these binary metal MXenes also show crystal structures, microscopic morphologies similar to the layered structures, gradually enriching the family of MXenes. MXenes exhibit various excellent properties due to their unique structures (*e.g.*, high electrical conductivity, good mechanical properties and hydrophilicity), which make them very attractive for battery and supercapacitor electrode material applications.[25]

The first member of the MXenes family, Ti_3C_2 MXene, was successfully prepared by Naguib's team by immersing Ti_3AlC_2 MAX phase in hydrofluoric acid solution (HF).[26] Subsequently, it was found that many other types of MXene family members could also be synthesized by selective etching of the A-layer in the MAX phase in HF.[27–31] With the increased interest in the study of MXene materials, many researchers have focused on MXene materials and theoretical chemists were able to predict new MXenes species by theoretical calculations.[32–34] In general, the M–X binding layer is relatively stable and the M–A binding layer exhibits relatively weak binding with respect to the M–X layer; therefore, selective reaction of the A-layer atoms with foreign particles and successive outward diffusion are the preferred strategies for creating M–X layer structures,[35] as shown in Fig. 1.

Interestingly, HF is the preferred etchant for the preparation of MXenes. Early studies showed that the MAX phase was inert in common acids (such as HCl, H_2SO_4 and HNO_3), common base solutions (NaOH) and common salts (NaCl and Na_2SO_4), none of which could achieve the stripping of the MAX phase. Finally, the M–A–X phase was immersed in dilute HF solution and successfully etched off the A layer selectively, and then two-dimensional MXene nanosheets were synthesized after delamination with the help of intercalating agents.[36,37] The synthesized MXene nanosheets are only a few atomic layers thick and similar to graphene and other two-dimensional materials,[38–40] so the two-dimensional transition metal carbon/nitrogen/carbon nitrides derived from MAX phase materials are called MXenes. The chemical general formula of MXenes is $M_{n+1}X_nT_x$ (*e.g.*, Ti_3C_2 MXene can also be written as $Ti_3C_2T_x$), where T_x is the surface functional group of MXenes (*e.g.*, O, F, and OH).[41]

Currently, hydrofluoric acid (HF) etching is the most widely used method for MXene preparation[42] and was used in the earliest preparation method. This method is simple to operate, easy to implement, and can be used to obtain more defects and

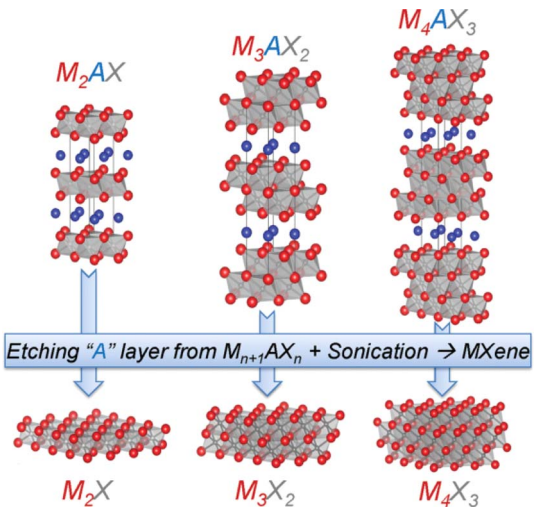

Fig. 1 Structures of MAX phases and their derived pristine MXene monosheets. M is a transition metal, *e.g.*, Ti; A is an element from group 13 or 14, *e.g.*, Al. X is C, N, or their combination.[24] Copyright 2013, Wiley-VCH.

smaller size MXene by increasing the acid concentration, extending the etching time, and increasing the temperature.[43] In addition to HF, LiF/HCl, NH_4HF_2, and other fluorides can achieve the same effect. In addition, MXene materials can be prepared by electrochemical etching, alkali-assisted etching, molten salt etching, anhydrous etching, and chemical vapor deposition (CVD).

There are many advantages of MXenes: in addition to high electrical conductivity, excellent ion migration rate, and good mechanical strength, they also have abundant surface functional groups and easy assembly properties.[44]

(1) The high density of electronic states near the Fermi energy level of most MXene exhibits high electronic conductivity, which can be widely used in electronic devices.

(2) Its low ion diffusion potential barrier brings fast ion migration rate, which is well suited as an electrode material for secondary batteries.

(3) In theoretical calculations, MXene has high mechanical strength, including hardness, bending stiffness, *etc.* Practical tests are usually performed using MXene films.

(4) MXene materials contain abundant surface functional groups that can form hydrogen bonds with water molecules, which can be dispersed in water or improve its aqueous solution wettability.[45] Its easy dispensability also makes it easy electrostatically self-assemble or compound with other materials, and the functional group species can be modulated according to the preparation method, which in turn affects its electrochemical properties. The functional group distribution can also be adjusted by high temperature annealing to reduce the content of –OH and –F.

(5) MXene surfaces are negatively charged and rich in reactive functional groups, and thus can be easily assembled into composites.[46]

3. MXene for the inhibition of lithium metal battery dendrites

Lithium-ion batteries are composed of cathode collector, cathode material, electrolyte (mass) and/or diaphragm, anode material, and anode collector. As an electrochemical energy storage device, lithium-ion batteries have the advantages of environmental friendliness, high specific energy, long cycle life, high output voltage, low self-discharge rate, and no memory effect, which make them the technology of choice for portable electronic devices, power tools, and hybrid/all-electric vehicles.[1,47,48] If electric vehicles powered by lithium-ion batteries replaced most gasoline-powered vehicles, greenhouse gas emissions would be greatly reduced. The high energy efficiency of lithium-ion batteries may also enable their use in a variety of grid applications, including improving the quality of energy harvested from wind, solar, geothermal, and other renewable sources, thus contributing to their wider use and promoting sustainable development. As a result, lithium-ion batteries have attracted strong interest from industry and government funding agencies, and researchers have conducted extensive research in this area in recent years.[1]

Lithium metal has a theoretical specific capacity of up to 3861 mA h g^{-1} and a very low redox potential (−3.040 V), resulting in a very high energy density of batteries with lithium metal as anode, which makes lithium metal one of the most promising anodes.[1] However, up to now, there are still a large number of challenges with lithium metal anodes, which seriously hinder its practical application.[4,49–54] Typical problems with lithium metal anodes, which are mainly including:

(1) Uneven lithium metal plating/stripping behavior during cycling can cause large volume expansion, reducing interfacial contact stability, leading to the generation of insulating "dead lithium" and reducing Coulomb efficiency.[55]

(2) The chemical and electrochemical reactivity of lithium metal is very strong, and lithium metal is prone to side reactions with the electrolyte, which will continuously consume the electrolyte and corrode the lithium, reducing the lithium metal utilization.[56]

(3) Lithium metal is prone to uncontrollable dendrite growth during cycling, and sharp dendrites may puncture the diaphragm, leading to short circuits, which may cause electrolyte combustion and trigger safety accidents such as battery explosions.[57]

(4) The loose and porous lithium dendrite deposition layer will slow down the diffusion rate of lithium ions and electrons, which makes the polarization increase. The loose lithium dendrites make the lithium metal surface area increase, which intensifies the occurrence of side reactions, which will seriously reduce the Coulomb efficiency.[58]

This set of problems not only make the cycle life of Li-metal batteries shorter, but also likely lead to safety hazards such as thermal runaway and Li-metal battery explosion and fire, which deprives Li-metal batteries of commercial market opportunities. Therefore, over the past 40 years, researchers have proposed many strategies to inhibit dendrite growth; however, up to now, solving these challenges for lithium metal anodes remains a long-term challenge.[15,56]

Recently, some important advances in the inhibition of lithium dendrite growth have been made by introducing MXene materials into Li-metal batteries.[59–67] MXene nanomaterials can provide nanoscale gaps and micropores for the lithium metal, resulting in uniform lithium stripping/deposition. Till now, MXene plays an important role in the following three aspects: (1) electrode materials of Li-metal batteries; (2) coating layer of Li metal anode, and (3) the skeleton of the three-dimensional (3D) composite anode.

3.1 MXene as electrode materials

Alkali metals are ideal anodes for high energy density rechargeable batteries, but they are constrained by their limited cycle life and low area capacity. Conductive carbon skeletons with good chemical stability and large surface area are often used as lightweight bodies for Li, but the poor lithophilicity of most carbon nanoskeletons leads to inhomogeneous nucleation/deposition processes and loose contact between Li and the collector fluid, which inevitably leads to Li dendrite formation and "dead Li" in subsequent cycles. This

phenomenon is more obvious at high current densities (>5 mA cm^{-2}). Therefore, the introduction of lithium-friendly materials on highly conductive carbon nanoskeletons is an urgent need to achieve highly lithium-loaded and dendrite free lithium metal anodes. 2D titanium carbide ($Ti_3C_2T_x$) has high electronic conductivity and lithium-friendly surface terminations (O, F, OH, Cl), making it an ideal building block for depositing 3D porous skeletons of alkali metals. However, conventional free-standing MXene films with dense nanosheets can only provide limited space to support the increasing capacity of alkali metals. In other words, designing a 3D lightweight, flexible, and conductive MXene support with high mechanical strength capability while achieving high current density and high capacity is an urgent need for alkali metal anodes.

MXene materials with metal infiltration properties construct a 3D skeleton that can effectively improve the deposition/exfoliation behavior of Li and Na, inhibit the growth of dendrites, and minimize the volume change of metal anodes. In addition, the MXene surface is rich in active functional groups and accompanied by excellent electrical conductivity, making it an excellent substrate material for the construction of electro-deposited alkali metals. These functional group sites can be

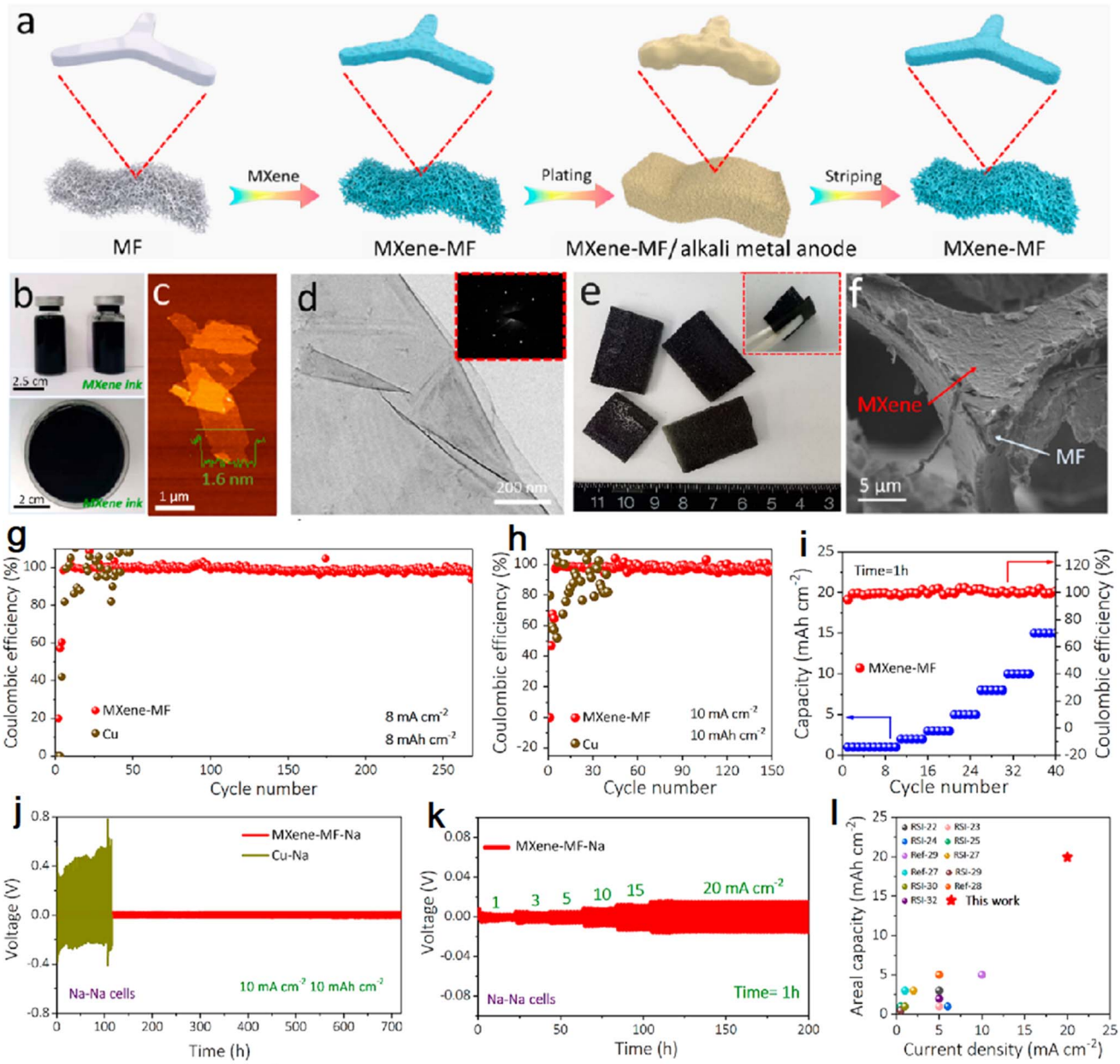

Fig. 2 (a) 3D MXene–MF fabrication process diagram; (b–d) photos, AFM and TEM images of MXene dispersion; (e and f) photos, SEM images of MXene–MF. (g and h) CEs of 3D MXene–MF and bare Cu electrodes; (i) CEs of MXene–MF and bare Cu electrodes with increasing current densities. (j) Galvanostatic cycling of symmetric cells based on MXene–MF–Na and Cu–Na electrodes. (k) Rate capability of symmetric cells based on MXene–MF–Na electrodes. (l) Comparison of areal capacity *vs.* current density of an MXene–MF–Na electrode with currently reported high areal capacity Na composite anodes. Reproduced with permission from ref. 59. Copyright 2020, American Chemical Society.

used as sites for electrodeposition to induce uniform lithium ion deposition.

The research team from Dalian Institute of Chemical Physics soaked melamine foam (MF) in MXene dispersion to obtain MXene skeletons with light mass, good flexibility, and excellent electrical conductivity.[59] The MXene–MF 3D interconnected porous conductive network with good mechanical flexibility and strength was obtained by using the high conductivity and lipophilic surface of MXene combined with the porosity, lightness and flexibility of 3D MF, which enables fast and uniform alkali metal deposition at high current density. Fig. 2a shows the 3D MXene–MF fabrication process. The high conductivity of MXene enhances the electron transfer rate and significantly reduces the metal ion concentration difference on the substrate surface. The lithium deposition process was observed under an optical microscope: a typical 3D porous structure was observed on the MXene–MF electrode, and the deposited surface was smooth and dense without dendrite formation and volume expansion during lithium deposition (Fig. 2f). In contrast, inhomogeneous lithium deposition with huge volume expansion was found in the bare copper electrode. The electrodeposition of lithium metal after soaking MXene effectively protects the mechanical strength of the melamine sponge and buffers the volume changes and internal stress fluctuations caused by metal deposition/exfoliation, maintaining the structural integrity of the electrode during high-power, deep alkali metal deposition/exfoliation.[60] The homogeneous conductivity of MXene and the large sheet structure increase the contact area between the electrode and the electrolyte and reduce the local current density. Fig. 2g–i shows the electrochemical performance of 3D MXene–MF for the Na anode.

A simple substrate comparison was performed by D. Yang's team in 2021:[61] the morphological evolution of the electrode with area capacity change (from 0.2 mA h cm^{-2} to 5.0 mA h cm^{-2}) and the morphological comparison after 300 cycles were characterized by scanning electron microscopy. Fig. 3a and n represent the lithium deposition on copper foil and $Ti_3C_2T_x$ substrate, respectively. The two substrates exhibit different lithium deposition behaviors. Initially, a small number of needle-like dendrites appear on the Cu foil (Fig. 3b) and grow with deposition, which indicates a tendency for continuous dendrite growth. When the deposition capacity reaches 5.0 mA h cm^{-2}, the Cu foil is covered with a large number of Li dendrites (Fig. 3d), while the Li growth on the $Ti_3C_2T_x$ substrate is planar and uniform (Fig. 3j). SEM images show that the Li deposition on the $Ti_3C_2T_x$ surface can be

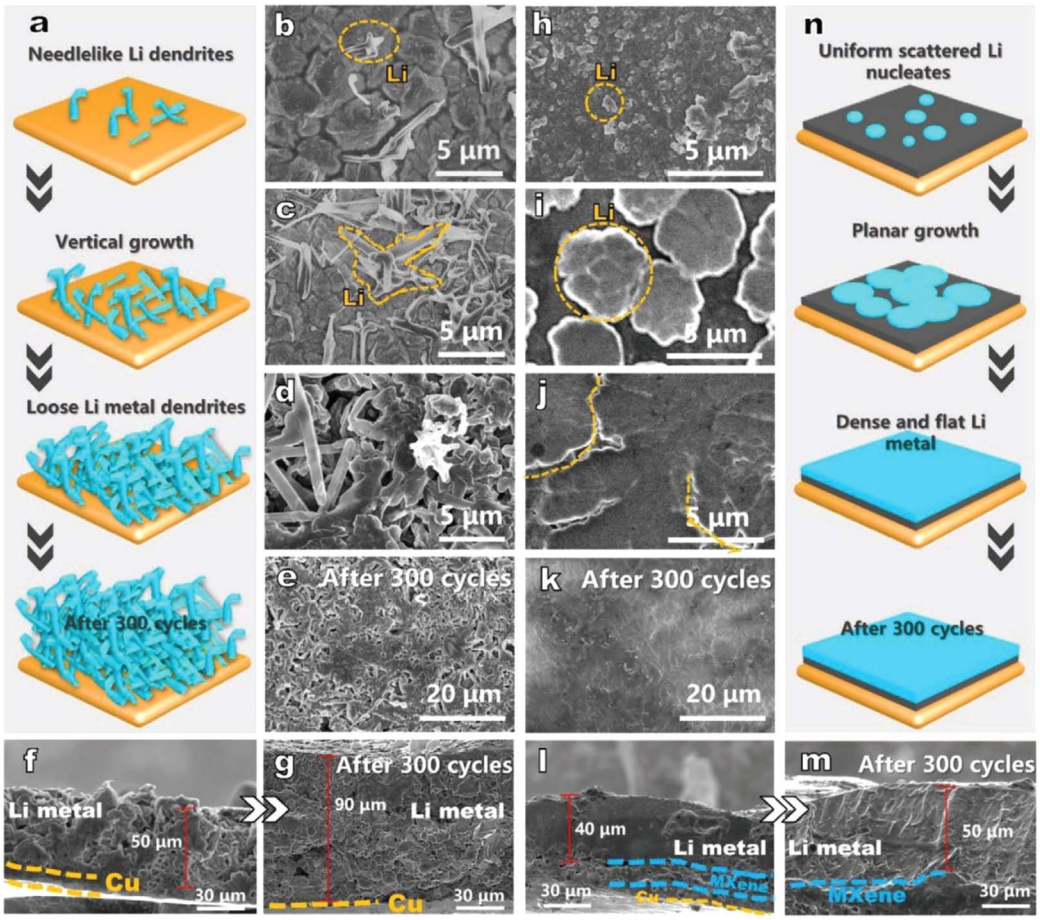

Fig. 3 Schematic representation of lithium deposition on (a) copper foil and (n) $Ti_3C_2T_x$ substrate; morphological evolution of (b–g) copper foil and (h–m) $Ti_3C_2T_x$. Reproduced with permission from ref. 61. Copyright 2021, Wiley-VCH.

divided into two stages. The first one is non-homogeneous nucleation, where Li nuclei of about 0.5 μm in diameter are formed on the $Ti_3C_2T_x$ surface (Fig. 3h). As Li continues to be deposited, the Li metal expands horizontally around the nucleus, forming smooth flat plates with a diameter of ≈5.0 μm (Fig. 3i). Next, uniform Li deposition was performed on these Li plates until a uniform and continuous Li film was formed on the $Ti_3C_2T_x$ substrate (Fig. 3j). But the biggest problem of the electrodeposition method is the electrodeposition process itself. For example, the lithium loss in the electrodeposition process is large, the morphology of the deposition process is not easily controlled, and the quality of the prepared Li electrodes usually cannot be guaranteed. Accordingly, this method can be improved by optimizing the electrodeposition process, such as using $Ti_3C_2T_x$ as the substrate for electrodeposition, adding complexing agents such as sodium citrate and surfactants such as SDS (sodium dodecyl sulfate) to the plating solution, in order to obtain a denser and uniform Li layer.[46]

3.2 MXene as coating layer of Li metal

In 2017, Prof. Yang's team at Peking University performed the first combination of MXene with lithium metal.[62] As shown in Fig. 4a, the article demonstrates a simple and effective strategy to first coat MXene on lithium plates, press them into thin sheets using a roller press, and repeat rolling after folding to further increase the number of layers of the hybrid plate while reducing the area of the hybrid plate. As the number of repetitions (n) increases, the thickness of lithium metal rapidly decreases while the number of lithium layers keeps increasing. In this way, the lithium metal is well confined in the gaps of the

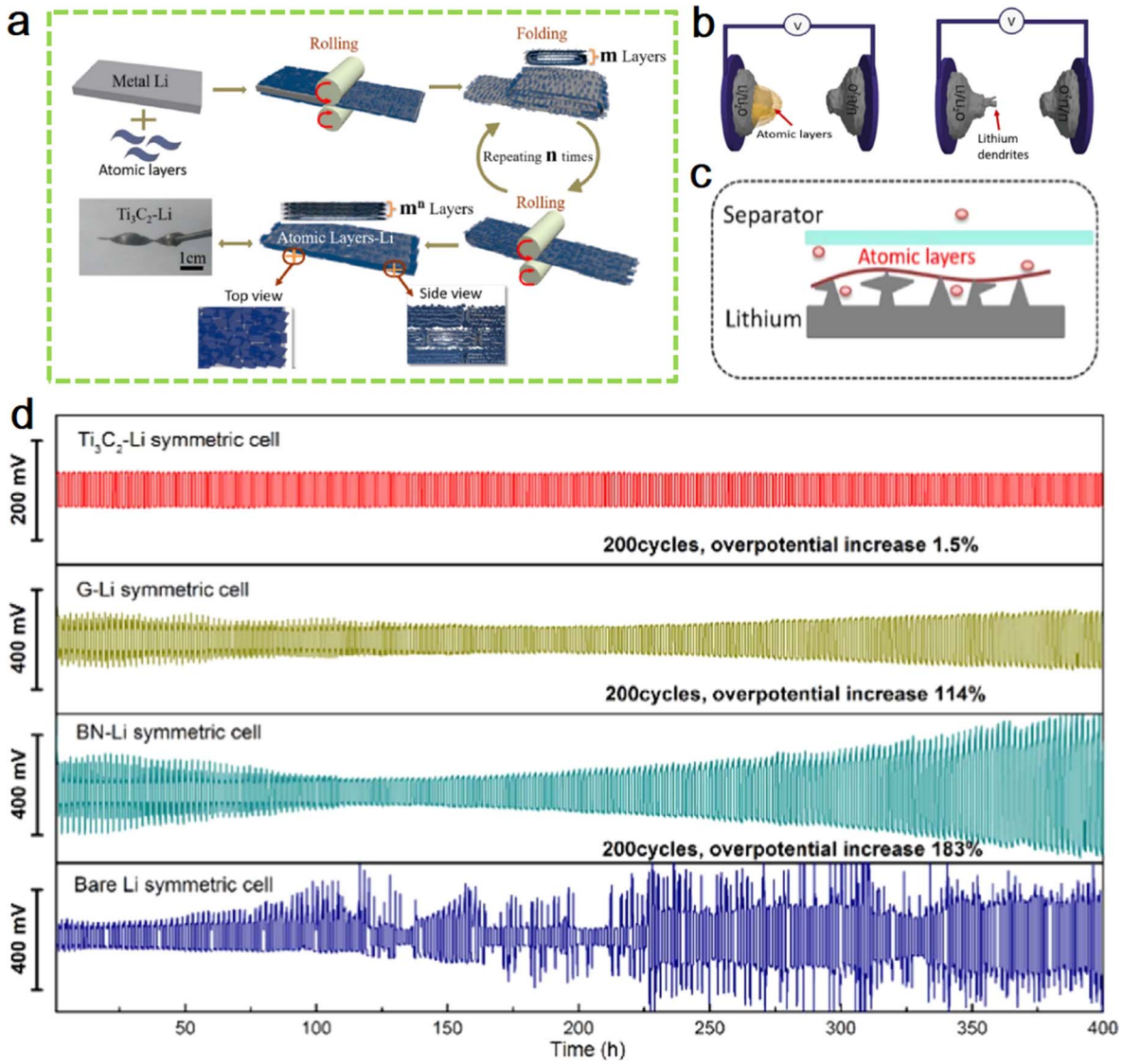

Fig. 4 (a) Schematic diagram of the preparation of flexible layered Ti_3C_2 MXene/lithium metal films. (b) The schematic illustration of the constructions of microcells with Ti_3C_2–Li (left) and bare Li (right) as working electrodes. (c) Schematic of the growing process of lithium dendrite in the presence of lithiophobic atomic layers. (d) Cycle performances of symmetric cells of Ti_3C_2–Li, G–Li, BN–Li and bare Li. Reproduced with permission from ref. 62. Copyright 2017, Elsevier.

MXene atomic layer. The advantage of this method is that the number of rolling and folding can be adjusted arbitrarily, producing alternating structures of lithium, MXene layers with adjustable number of layers. The layered MXene film becomes an effective barrier to lithium dendrites, allowing the electrode to exhibit excellent cycling stability. Fig. 4b schematically exhibits the comparison of Ti_3C_2–Li and bare Li as working electrodes. More importantly, the excellent electrical conductivity and complex functional groups of the MXene layer can induce lithium deposition in its interstices during the lithium metal deposition exfoliation process, and the robust MXene layer can also provide an effective protective barrier for the growth of lithium metal dendrites. Fig. 4c shows the growing process of lithium dendrite in the presence of lithiophobic atomic layers. The conductive Ti_3C_2 MXene enables controlled growth of lithium dendrites in nanoscale gaps, preventing their vertical growth from piercing the septum. Fig. 4d shows cycle performances of symmetric cells of Ti_3C_2–Li, G–Li, BN–Li and bare Li.

However, it need to be exposed MXene and lithium sheets in the glove box for a large area and a long time using this method, which may react with the residual air in the glove box and affect their interfacial contact properties. Limited by the long operation time, the lithium sheet is easy to oxidation, can try to add the appropriate amount of electrolyte during the rolling process, on the one hand, to reduce the oxidation reaction, on the other hand, can accelerate the contact reaction between MXene and lithium sheet.

In addition to repeat rolling, a simple one-shot rolling method can be used to embed MXene layers onto lithium wafers. Professor John Niu's team at the University of Wisconsin first coated MXene on a copper foil, and then rolled the copper foil together with the lithium wafer to obtain an MXene film-protected lithium wafer.[63] Fig. 5a–d show the atomic structure and morphology of $Ti_3C_2T_x$ MXene. Fig. 5e shows the fabrication process of MXene–Li electrode. During the deposition/exfoliation process, the large surface area and expandability of MXene provide enough space for lithium storage, as shown in Fig. 5g–i. The high electrical conductivity and abundant functional groups of MXene promote fast ion and electron transport. Meanwhile, the two-dimensional spatial potential limitation effect of MXene layer further inhibits the formation of dendrites.

3.3 MXene as the skeleton of the 3D composite anode

Alkali metals have low melting points, 180, 97.7, and 63.6 °C for lithium, sodium, and potassium, respectively.[64] Based on this property, molten alkali metals can be infused into three-dimensional or two-dimensional MXene materials. Cao Dianxue's team obtained alkali metal electrodes by infusing molten lithium and sodium metals into rGO (reduced graphene oxide)/$Ti_3C_2T_x$ composite films.[65] First, dense $Ti_3C_2T_x$–GO films were prepared by filtering a homogeneous colloidal mixture of few layers of $Ti_3C_2T_x$ and GO (graphene) nanosheet dispersions. Then, the $Ti_3C_2T_x$–GO films were contacted with the hot bench

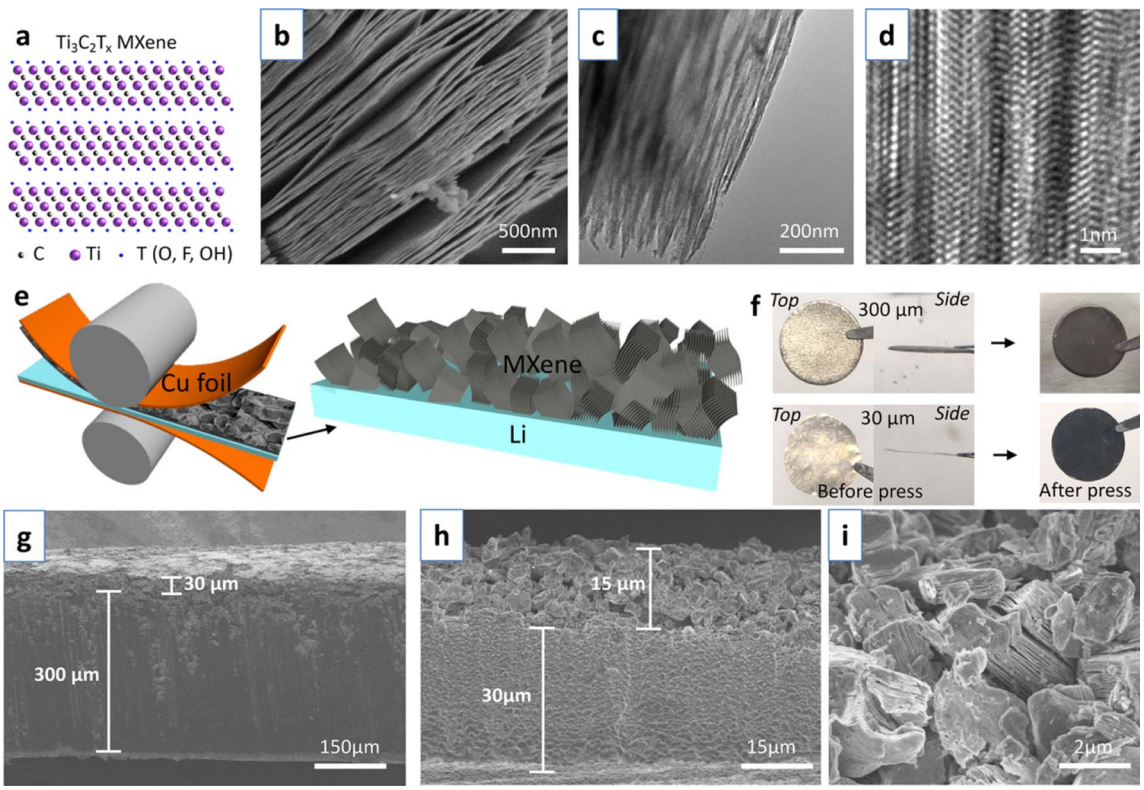

Fig. 5 (a–d) Atomic structure, SEM, TEM, and high-resolution images of $Ti_3C_2T_x$ MXene; (e) fabrication process of MXene–Li electrode; (f) digital photographs of lithium sheets; (g–i) SEM images of MXene–Li electrode.[63] Copyright 2020, American Chemical Society.

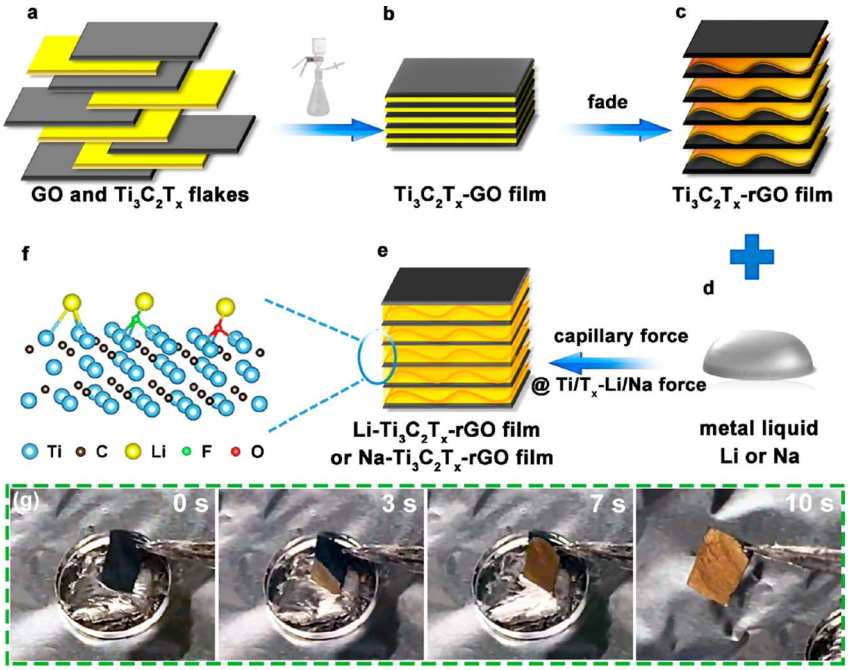

Fig. 6 (a–f) Schematic diagram of Li/Na–$Ti_3C_2T_x$–rGO preparation; (g) wetting process of $Ti_3C_2T_x$–rGO.[65] Copyright 2019, American Chemical Society.

or molten lithium metal and underwent a "fading reaction", which was visible as a darkening of the color (Fig. 6g). This is caused by the removal of water molecules and oxygen-containing functional groups from the $Ti_3C_2T_x$ layer. In this process, the graphene oxide reduces itself to form rGO. The removal of oxygen-containing functional groups from graphene oxide generates gas, which leads to interlayer micro-explosion and widens the layer spacing. After that, the $Ti_3C_2T_x$–GO film becomes a $Ti_3C_2T_x$–rGO film with a porous structure. Finally, the prepared films were injected with molten alkali metals (Li or Na) to obtain alkali metal electrodes (Fig. 6a–f). The molten metal flows rapidly and is wrapped in the porous $Ti_3C_2T_x$–rGO films under the effect of capillary forces generated by the uniform nano-gaps and the wettable surface of $Ti_3C_2T_x$. $Ti_3C_2T_x$ has low adsorption energy for Li and Na (−0.705, −1.0464 eV); similarly, the F- and O-containing functional groups exhibit good adsorption ability for Li and Na (F–Li, F–Na, O–Li and O–Na at −0.615, −1.0594, −0.931, −1.0144 eV, respectively). This result can provide a theoretical basis for the subsequent preparation and stable deposition stripping of $Ti_3C_2T_x$ based lithium and sodium metal cathodes. This method makes good composite use of two-dimensional materials, graphene and MXene, and is highly operable and can be widely applied to alkali metal batteries, such as Na batteries and Zn batteries, with high potential value.

Thanks to the uniform capillary force between the film layers and the wettable surface of $Ti_3C_2T_x$, the molten metal will rapidly flow into and be encapsulated into the multilayer $Ti_3C_2T_x$–GO film. However, the melt infusion method requires a large amount of heat to melt the alkali metal, and the melting process makes the alkali metal more susceptible to oxidation and increases the risk of handling in a glove box. A combination of tumbling and melt infusion can be tried by physically tumbling MXene with the alkali metal to achieve a certain degree of homogeneous mixing. This is followed by the melt method, which effectively improves the homogeneity of the mix while lowering the melt temperature.

Compared to 2D MXene, the porous 3D MXene backbone enables higher lithium loading.[66,67] 3D lightweight scaffolds are well suited for melt infusion of lithium metal, increasing the active lithium content and minimizing the volume change of the lithium cathode during stripping/deposition. Secondly, the interconnected porous conducting skeleton structure significantly reduces the local current density and delays the lithium dendrite growth rate. The well-dispersed lithium-loving MXene nanosheets allow for a uniform distribution of the electric field, and lithium is able to nucleate and grow uniformly across the framework rather than on the top surface of the electrode. As a result, the formation of lithium dendrites was greatly inhibited.

4. MXene for the inhibition of zinc metal battery dendrites

In the past three years, researchers have applied MXene to the anode of zinc metal batteries and zinc ion hybrid capacitors, respectively, and made a series of important advances in the inhibition of zinc dendrite growth,[68–71] mainly in three aspects: (1) MXene modification on the surface of zinc metal;[72–80] (2) MXene as an electrolyte additive;[81–84] and (3) structural optimization of the MXene/zinc composite.[85–91]

4.1 Zinc metal surface modification

MXene is modified on the metallic Zn surface to form a protective layer to inhibit Zn dendrite formation. In 2021, Niu *et al.* of Nankai University[72] proposed an *in situ* spontaneous reduction/assembly strategy to assemble ultrathin and uniform $Ti_3C_2T_x$ MXene layers on the Zn negative electrode surface, as shown in Fig. 7a. Compared with pure Zn, the MXene layers containing –OH, –O, and –F groups give the Zn negative electrode a lower nucleation potential barrier and a more uniformly distributed electric field through a good charge redistribution effect (Fig. 7b and c). Meanwhile, the wettability between the functionalized MXene layer and the electrolyte is stronger than that of the unmodified Zn, which contributes to the penetration of the electrolyte. The contact angles of electrolyte on pure Zn foil and MXene-coated Zn are shown in Fig. 7e. Therefore, the MXene modified Zn anode exhibits good stability of dendrite free cycling, mainly because the modulation of Zn^{2+} by oxygen-containing hydrophilic groups effectively inhibits the growth of Zn dendrites (Fig. 7c and d).

In 2022, Zhi *et al.*[73] further developed a series of highly lattice-matched iso-chemical stoichiometric halogenated MXene as artificial interfacial layers through the introduction of halogen-functional MXene–Zn ($Ti_3C_2Br_2Zn$, $Ti_3C_2Cl_2Zn$, $Ti_3C_2I_2Zn$) composite Zn metal anodes, and found that halogenated MXene induced highly reversible, homogeneous deposition of Zn ions, indicating that the non-hydrophilic halogen groups were also able to guide the homogeneous deposition of Zn and avoid the formation of Zn dendrites. Fig. 8 shows Zn plating/stripping behavior in symmetric batteries based on bare Zn metal, Ti_3C_2OF–Zn, $Ti_3C_2Cl_2$–Zn, $Ti_3C_2Br_2$–Zn, and $Ti_3C_2I_2$–Zn anodes. It was also found that different halogen (F, Cl, Br and I) functionalized MXene have different effects on inhibiting Zn

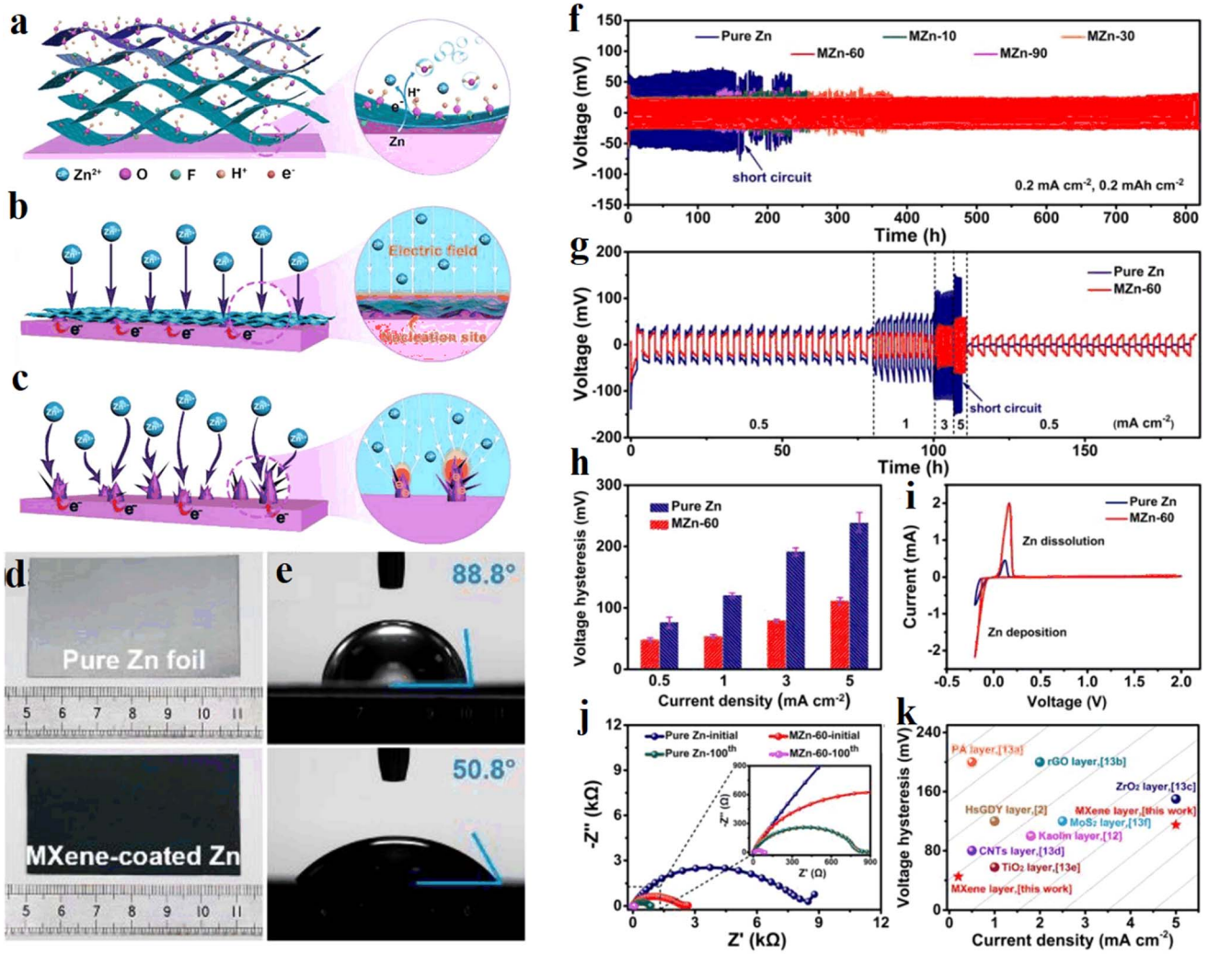

Fig. 7 (a) Schematic illustration of the assemble of MXene layer on Zn foil. (b and c) Schematic exhibition of Zn plating behavior of (b) MXene-coated Zn and (c) pure Zn. (d) The morphology of pure Zn foil and MXene-coated Zn. (e) Contact angles of electrolyte on pure Zn foil and MXene-coated Zn. (f) Long-term cycling performance at 0.2 mA cm^{-2}. (g) Rate performance, and (h) the corresponding voltage hysteresis at different current densities. (i) CV curves of Zn plating/stripping. (j) Nyquist plots of symmetric cells using pure Zn and MZn-60 before cycling and after 100 cycles. (k) Comparison of voltage hysteresis of a MZn-60 anode with some previously reported anodes with different coating layers. Reproduced with permission from ref. 72. Copyright 2021, Wiley-VCH.

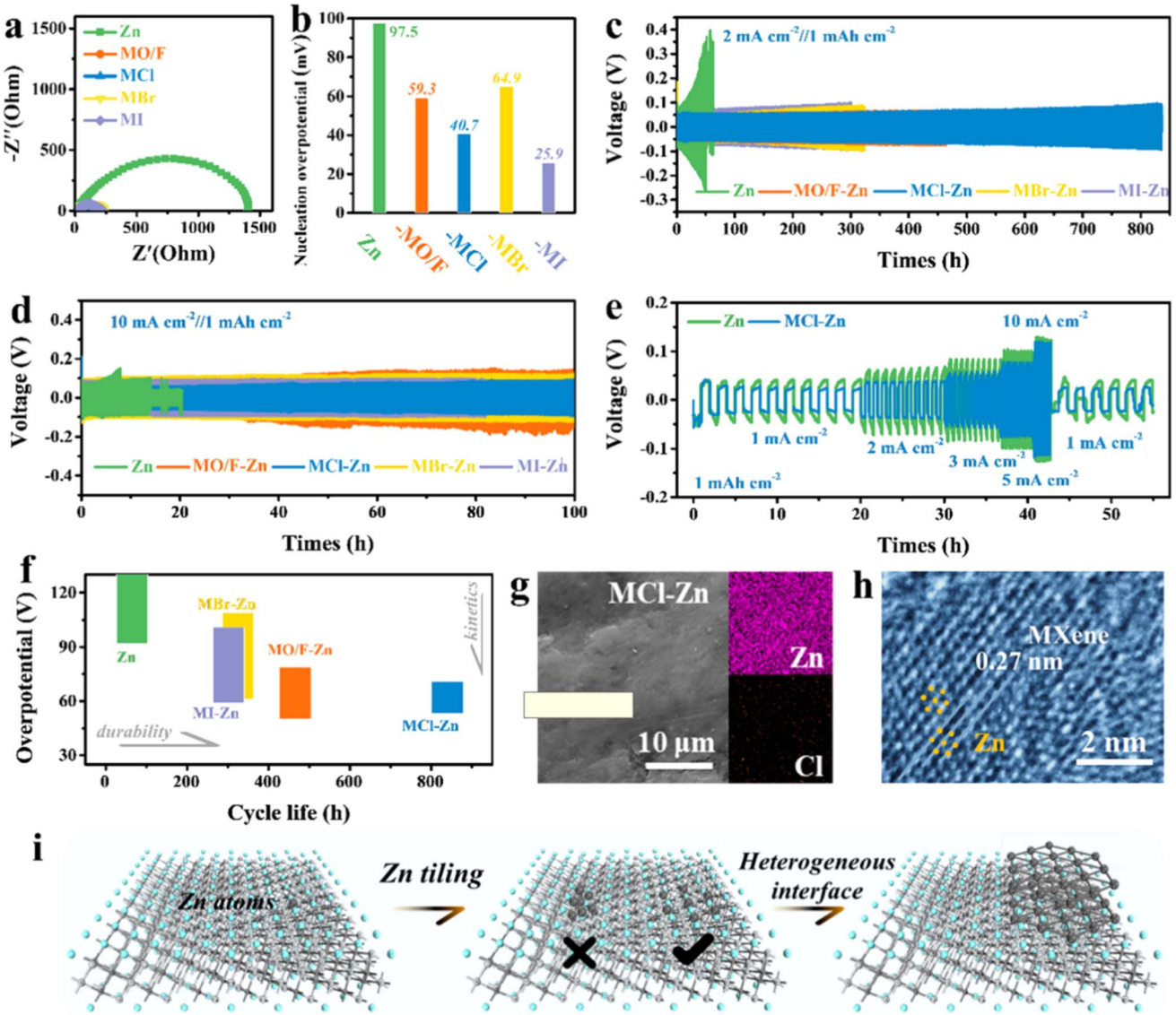

Fig. 8 Zn plating/stripping behavior in symmetric batteries based on bare Zn metal, Ti_3C_2OF–Zn, $Ti_3C_2Cl_2$–Zn, $Ti_3C_2Br_2$–Zn, and $Ti_3C_2I_2$–Zn anodes. (a) Electrochemical impedance spectra of the symmetric batteries. (b) Nucleation overpotential of the symmetric batteries. (c) Long-term cyclic performance of symmetric batteries at 2 mA cm^{-2}. (d) Long-term cyclic performance of symmetric batteries. (e) Comparison of voltage profiles during Zn stripping/plating of bared Zn metal and $Ti_3C_2Cl_2$–Zn symmetric batteries. (f) Comparison of cycle durability and overpotential. (g) SEM images and EDX mapping of the MCl–Zn electrode after cycling. (h) HRTEM image of the heterointerface region with the coexistence of the $Ti_3C_2Cl_2$ matrix and Zn deposits. (i) Schematic illustration of the Zn deposition process. Reproduced with permission from ref. 73. Copyright 2021, American Chemical Society.

dendrite growth, among which $Ti_3C_2Cl_2$ and $Ti_3C_2F_2$ containing –Cl and –F functional groups have the best effect on inhibiting Zn dendrite, showing the key role played by the functional group type, which provides a new idea for the development of high-safety Zn electrodes.

Except for instability, Zn metal also has high thermodynamical activity in aqueous electrolytes, which can ignite a series of side reactions and accelerate the electrode corrosion. To overcome this problem, an interesting work was reported by Bin Xu *et al.* in 2023.[74] They prepared a Cu-modified $Ti_3C_2Cl_2$ MXene (Cu–MXene) with high zincophilic and hydrophobic property using a one-step molten salt etching method and coated it on the Zn anode. The fabrication process was schematically illustrate in Fig. 9a. Compared with bare Zn, MXene–Zn, Cu–MXene has stronger wettability to the electrolyte (Fig. 9b). Moreover, the hydrophobic coating can prevent the Zn anode from the aqueous electrolyte, beneficial for suppressing the side reactions, as illustrated in Fig. 9c. As a result, the Zn anode coated by the Cu–MXene shows excellent plating/stripping behavior (Fig. 9d–f) and cycling performance (Fig. 9g and h). The simply prepared Cu–MXene coating was predicted can be extended to other energy storage systems due to its easy fabrication and low cost. Another interesting work in this field was reported by Zhang *et al.* in this year.[75] They coated a layer of polyvinylidene fluoride (PVDF)-based PVDF–MXene on Zn metal using 3D printing technology. The fabrication process was

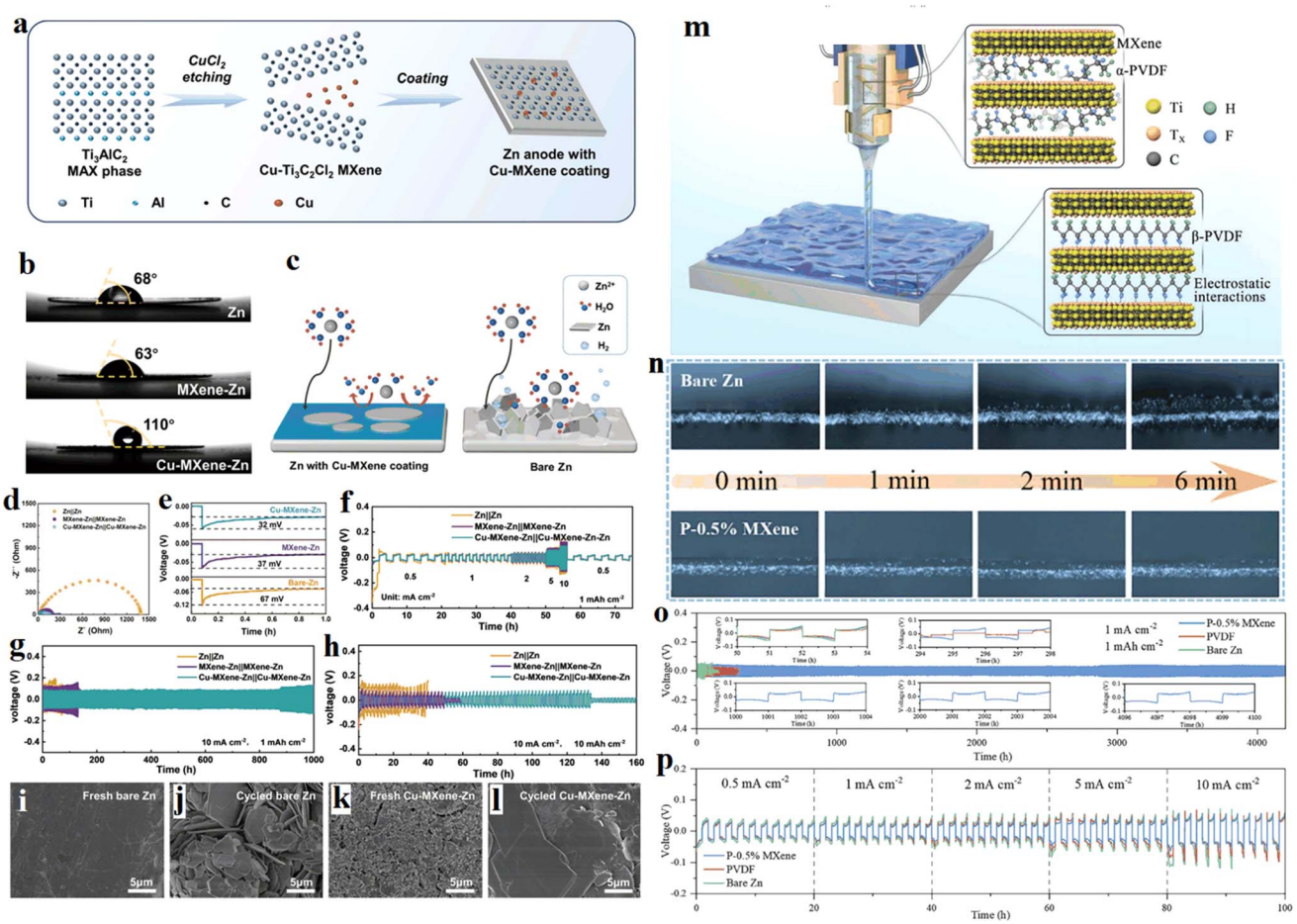

Fig. 9 (a) Schematic illustration of Zn electrode with Cu–MXene coating. (b) Contact angles of $ZnSO_4$ electrolyte on bare Zn, MXene–Zn, and Cu–MXene–Zn foils. (c) Illustration of the inhibition on side reactions of Cu–MXene hydrophobic coating on Zn. (d–f) Zn plating/stripping behavior in symmetric cells based on bare Zn, MXene–Zn, and Cu–MXene–Zn electrodes. (g and h) Cycling performance at 10 mA cm^{-2} with a real capacity. (i–l) SEM images of bare Zn and Cu–MXene–Zn electrode before and after cycling. Reproduced with permission from ref. 74. Copyright 2023, Wiley-VCH. American Chemical Society. (m) The fabrication process and mechanism of the PVDF–MXene artificial protective layer on Zn metal with 3D printing technology. (n) *In situ* optical microscopy images of Zn plating on bare zinc foil and P–0.5% MXene coated zinc foil. (o) Galvanostatic Zn plating/stripping cycling performance. The insets show the enlarged voltage profiles at different cycling hours. (p) Rate performance of symmetric cells. Reproduced with permission from ref. 75. Copyright 2024, Wiley-VCH.

shown in Fig. 9m. The ferroelectric properties of the printed PVDF films was enhanced due to the phase transition of the PVDF polymer chains, and thus an effective manipulation of the PVDF films to the zinc ions was realized. Zinc ions are concentrated on the surface of the ferroelectric protective layer, promoting the uniform deposition of zinc and prolongs the cycle life of the symmetrical cell. From Fig. 9n, the *in situ* optical microscopy images of Zn, there are amount of Zn dendrites grown up on bare zinc foil, while no Zn dendrite was found on the P–0.5% MXene coated zinc foil. The symmetrical zinc batteries using PVDF–MXene–Zn anode exhibit reversible Zn plating/stripping, high-rate capability enhanced cycling stability (Fig. 9o–p).

However, the above studies are still controversial in terms of the explanation of the mechanism of action of hydrophilic and non-hydrophilic functional groups of MXene in inhibiting zinc dendrites, mainly because of the differences in the modulation of zinc diffusion and deposition behavior by different types and distributions of functional groups.

4.2 MXene as an electrolyte additive

The growth of zinc dendrites was also inhibited by using MXene as an additive to the electrolyte. MXene acts as an additive to aqueous electrolytes (or collectors) to optimize the deposition location of zinc ions, promote uniform deposition of zinc ions, and inhibit dendrites. Wang *et al.* from Jiangsu Normal University[81] added a small amount of $Ti_3C_2T_x$ MXene nanosheets to the liquid electrolyte (2 M $ZnSO_4$).The $Ti_3C_2T_x$ additive formed a stable solid electrolyte interface (SEI) protective film on the zinc negative surface, and the abundant functional groups on $Ti_3C_2T_x$ and its own excellent electrical conductivity could effectively induce the metallic zinc. This further demonstrates the important role of $Ti_3C_2T_x$ MXene containing –OH, –O, –F functional groups on Zn dendrites, and the addition

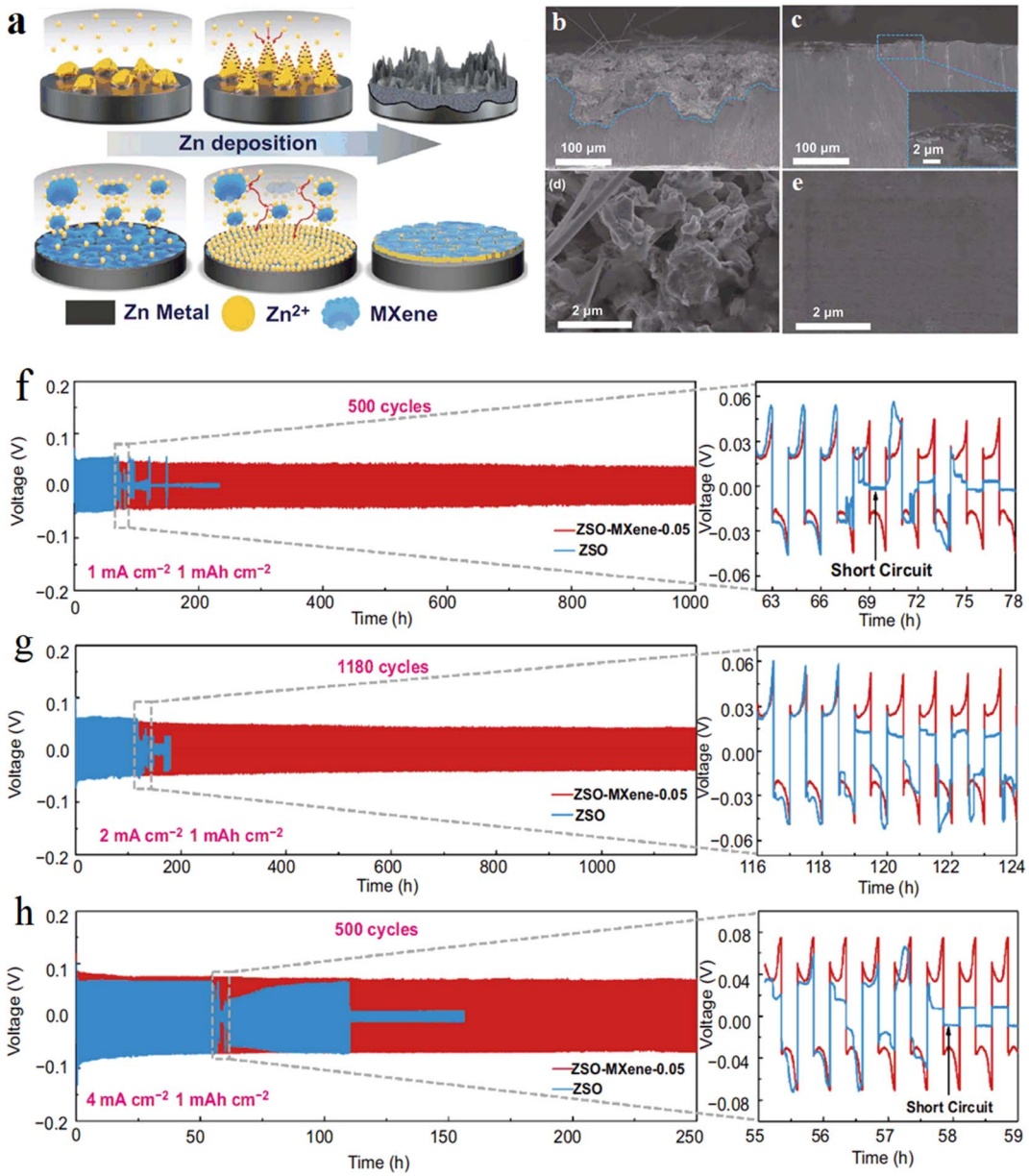

Fig. 10 (a) Schematic illustration of the effect of MXene additive on the Zn deposition process. (b–e) Cross-sectional and surface configuration of Zn anode after cycling at current density of 2 mA cm^{-2} with 1 mA h cm^{-2} Zn plating/stripping: (b) and (d) in ZSO electrolyte after 50 h, (c) and (e) in ZSO–MXene-0.05 electrolyte after 50 h. (f–h) Long-term galvanostatic cycling of Zn–Zn symmetrical cell at 1, 2 and 4 mA cm^{-2} with the capacity of 1 mA h cm^{-2}. Reproduced with permission from ref. 81. Copyright 2021, The Authors.

amount should be strictly controlled due to the high electrical conductivity of MXene (Fig. 10).

The solid polymer electrolyte PVHF/MXene-*g*-PMA was prepared by Chunyi Zhi's group[82] using poly(methyl acrylate) (PMA) grafted MXenes to fill poly(vinylidene fluoride)-*co*-hexafluoropropylene (PVHF). Due to the interaction between the highly grafted PMA and PVHF matrix, the MXenes were uniformly dispersed and highly reversible dendrite free Zn deposition/exfoliation. These studies provide implications for the design of novel electrolyte materials, but the formation process and evolutionary mechanism of SEI at the electrode/electrolyte interface under the action of MXene is unknown (Fig. 11).

4.3 Structural optimization of the MXene/zinc composite

Structural optimization was performed to construct three-dimensional (3D) MXene/Zn negative composites based on the host design of MXene to inhibit the formation of Zn dendrites by shortening the Zn ion diffusion/deposition path. By designing heterostructures of electron-conducting 3D sulfur-doped MXene and ion-conducting ZnS, researchers Feng *et al.* from Shandong University[85] used sulfur-doped MXene to induce uniform distribution of electric field, reduce local current density, and buffer volume changes. Fig. 12a shows the fabrication process of S/MX@ZnS@Zn at different temperatures schematically. The growing ZnS not only effectively inhibits the

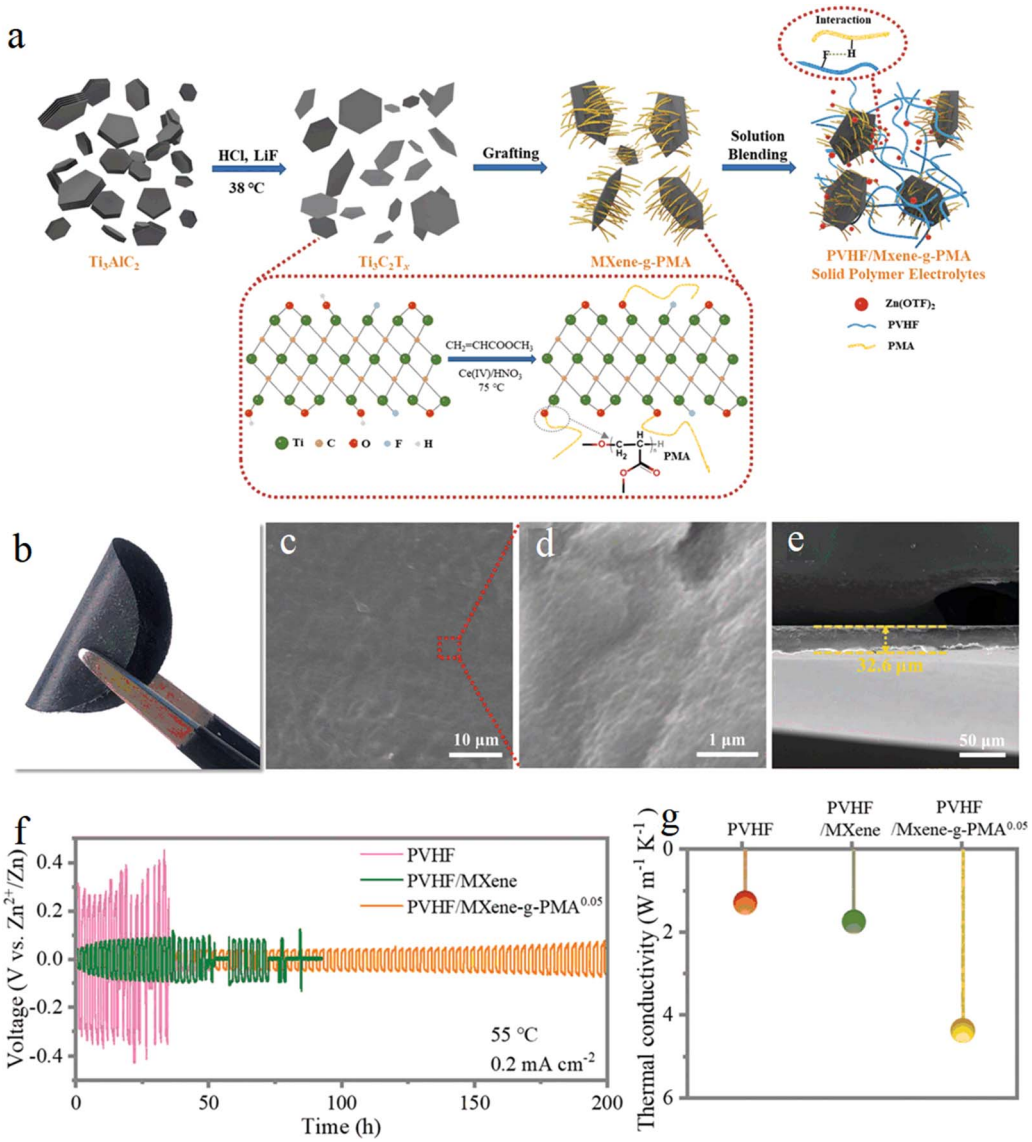

Fig. 11 (a) Schematic illustration of the overall preparation process of the SPEs. (b) Optical picture; (c) and (d) SEM images of the surface; (e) SEM of the cross-section; (f) galvanostatic Zn plating/stripping in the Zn/Zn symmetrical cells based on the as prepared SPEs; (g) thermal conductivity of the as-prepared SPEs. Reproduced with permission from ref. 88. Copyright 2021, The Royal Society of Chemistry.

growth of Zn dendrites and the occurrence of side reactions, but also promotes the uniform distribution and accelerates the transfer of Zn ions, resulting in a large improvement in the performance of Zn energy storage devices (Fig. 12b–d). Chen *et al.* from Beijing University of Technology[86] constructed a 3D flexible $Ti_3C_2T_x$ MXene/graphene scaffold by using the directional freezing method, and zinc ions were densely wrapped inside the 3D scaffold body through the electrodeposition process, which not only effectively suppressed dendrite growth, but also inhibited hydrogen precipitation reaction and zinc passivation, providing a new idea for the construction of stable 3D zinc-based anode. Fig. 12e schematically illustrates the fabrication of MXene and graphene aerogel (MGA). Fig. 12f and g shows the morphology of the MGA material. Long-cycling performance of symmetric cells using Cu@Zn and MGA@Zn electrodes was compared in Fig. 12h. Form Fig. 12i and j, the superiority of the MGA@Zn electrodes can be observed through the comparison of the size of the zinc dendrites.

A research team from Soochow University[87] proposed a generalized divalent cation-assisted gelation strategy to prepare 3D printed additive-free Ti_3C_2 MXene ink with good rheological properties, and the formation of this gel could effectively inhibit the re-stacking of MXene nanosheets by assembling 3D printed prepared MXene cathodes and CNT/Zn anodes into zinc ion hybrid capacitors, uniform electrodeposition of Zn on 3D printed CNT structures suppressed Zn dendrite formation. The relevant results can be found in Fig. 13a–f. Based on the easy oxidation of MXene, Li's team[88] evolved a series of 3D alkalized MXene/metal (AMX–M, M is Cu, Zn and Ag, *etc.*) composites with special morphology by hydrothermal alkalinization and metal ion pre-intercalation of 2D $Ti_3C_2T_x$ MXene. The synthesis mechanism of AMX-derived composite

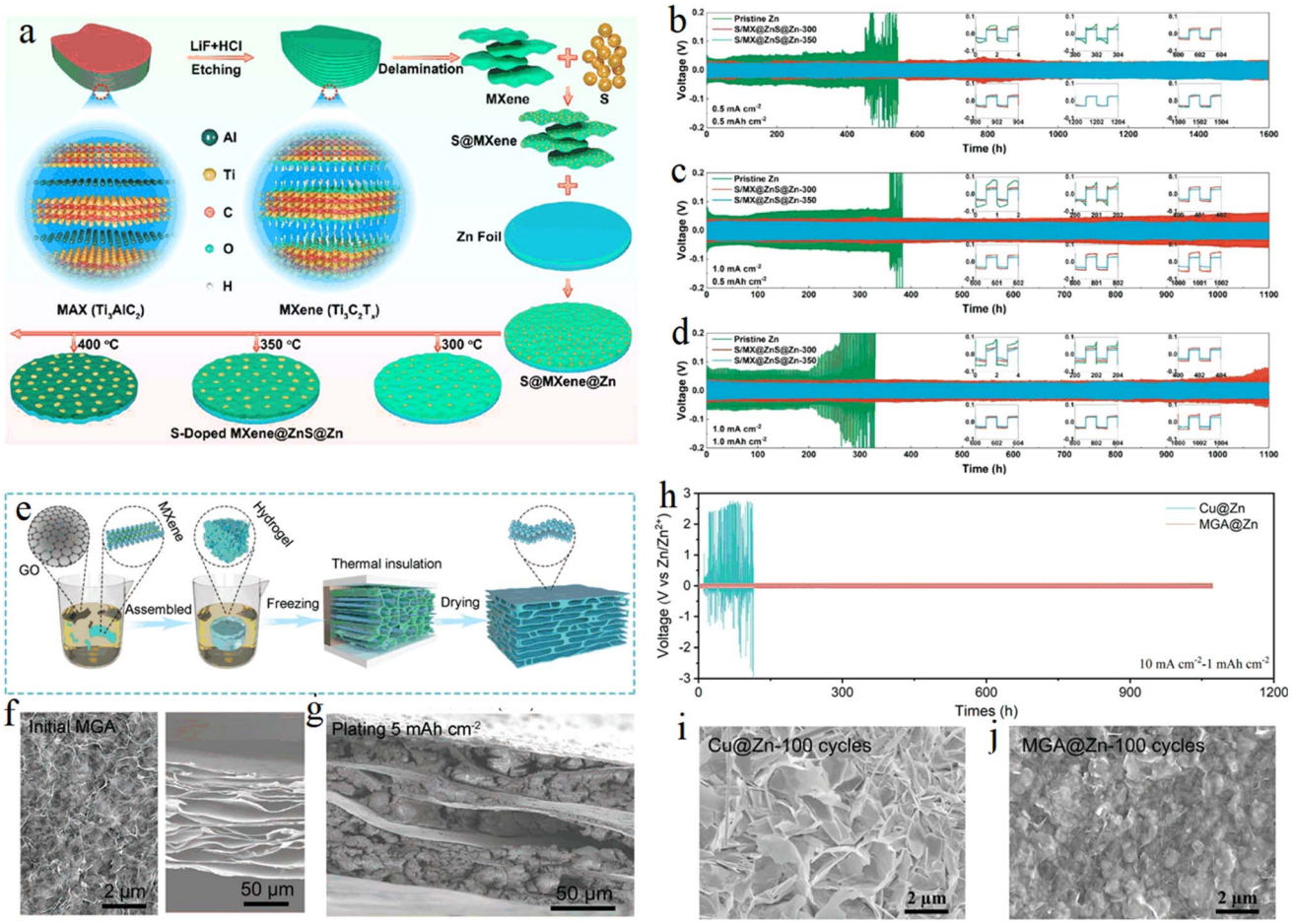

Fig. 12 (a) Schematic illustration of fabrication of S/MX@ZnS@Zn at different temperatures. (b–d) Cycling performance at various rates and area capacities of (b) 0.5 mA cm^{-2} to 0.5 mA h cm^{-2}, (c) 1.0 mA cm^{-2} to 0.5 mA h cm^{-2}, and (d) 1.0 mA cm^{-2} to 1.0 mA h cm^{-2}. Reproduced with permission from ref. 85. Copyright 2021, American Chemical Society. (e) Schematic illustration of fabricating MGA material. (f) SEM images of top (left) and side views under unconstrained conditions for the MGA material. (g) Side-view image. (h) Long-cycling performance of symmetric cells using Cu@Zn and MGA@Zn electrodes. (i and j) Top-view SEM images of Cu@Zn (i) and MGA@Zn (j) electrodes. Reproduced with permission from ref. 86. Copyright 2021, Wiley-VCH.

was shown in Fig. 13g. Among them, 3D MXene derivatives and Zn composites obtained by pre-intercalation of Zn ions are used to replace the conventional zinc foil anode assembled with porous carbon to form zinc ion hybrid capacitors. The results show that the energy density of the assembled Zn ion capacitor is substantially improved compared to the conventional asymmetric energy storage device. After 10 000 charge/discharge cycles, the energy storage device still maintained an excellent initial specific capacity of 92.5%, showing a cycle life much higher than that of pure MXene and pure Zn metal electrodes (Fig. 13h). It was shown that $Ti_3C_2T_x$ derivatives applied to zinc energy storage devices could effectively inhibit the growth of zinc dendrites and improve the reversibility of zinc ions, but difficulties arose in explaining the mechanism of dendrite growth inhibition by MXene derivatives.

In last year, Zhang and his team[89] reported a design concept of 3D artificial array interface engineering to achieve volume stress elimination, preferred orientation growth and dendrite-free stable Zn metal anode. Fig. 14a shows the fabrication process of 3D MXene array@Zn. The researchers explored how the MXene array interface modulates the deposition of Zn atoms using various spectral techniques and theoretical calculations. In addition, the electrochemical performance tests support their conclusion well that the engineered electrode can enhance the rate capability and cyclic stability of the Zn metal anode, as shown in Fig. 14b–f.

In this year, Liu and his team[90] reported a flexible Zn anode using highly conductive Ti_3C_2 MXene coated nylon fabric (MXNY) as a three-dimensional Zn deposition skeleton. In this work, polydopamine (PDA) was used as a solid electrolyte interface (SEI). Synergistic benefits, such as a stabilized interface, donated by MXNY and PDA SEI bring homogeneous Zn deposition and higher corrosion resistance to the zinc anode. As a result, improved coulombic efficiency and long cycling stability was achieved in the present flexible and stable Zn anode. Fig. 14g–j shows the morphology of Zn deposition on highly aligned MXene (HLMX), without and with DA additive. The cycling stability of symmetric MXNY@Zn cells was shown in Fig. 14k–p.

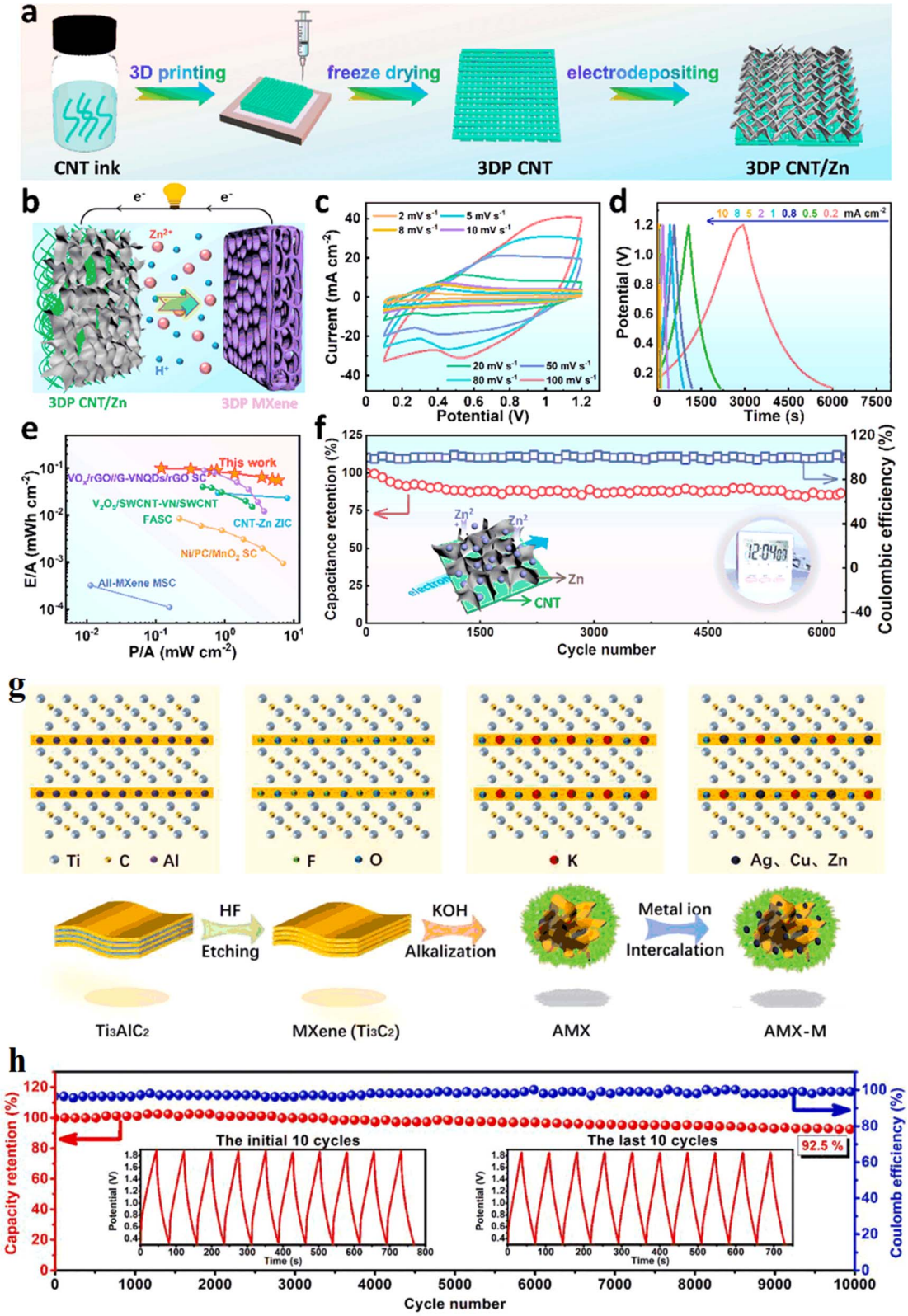

Fig. 13 (a) Schematic diagram showing the preparation process of the 3DP CNT/Zn anode. (b) Schematic diagram showing the discharging process of the 3DP ZIC full cell. (c) CV profiles of the 3DP ZIC full cell at a scan rate from 2 to 100 mV s^{-1}. (d) GCD curves of the 3DP ZIC at different current densities. (e) Ragone plots of our 3DP ZIC in comparison with other reported printable energy storage devices. (f) Cycling performance of the 3DP ZIC full cell at 10 mA cm^{-2}. Reproduced with permission from ref. 87. Copyright 2021, American Chemical Society. (g) Synthesis mechanism of AMX-derived composite. (h) Specific capacitance and coulombic efficiency of the AMX-ZIS as a function of GCD cycle number. Reproduced with permission from ref. 88. Copyright 2021, Elsevier B.V.

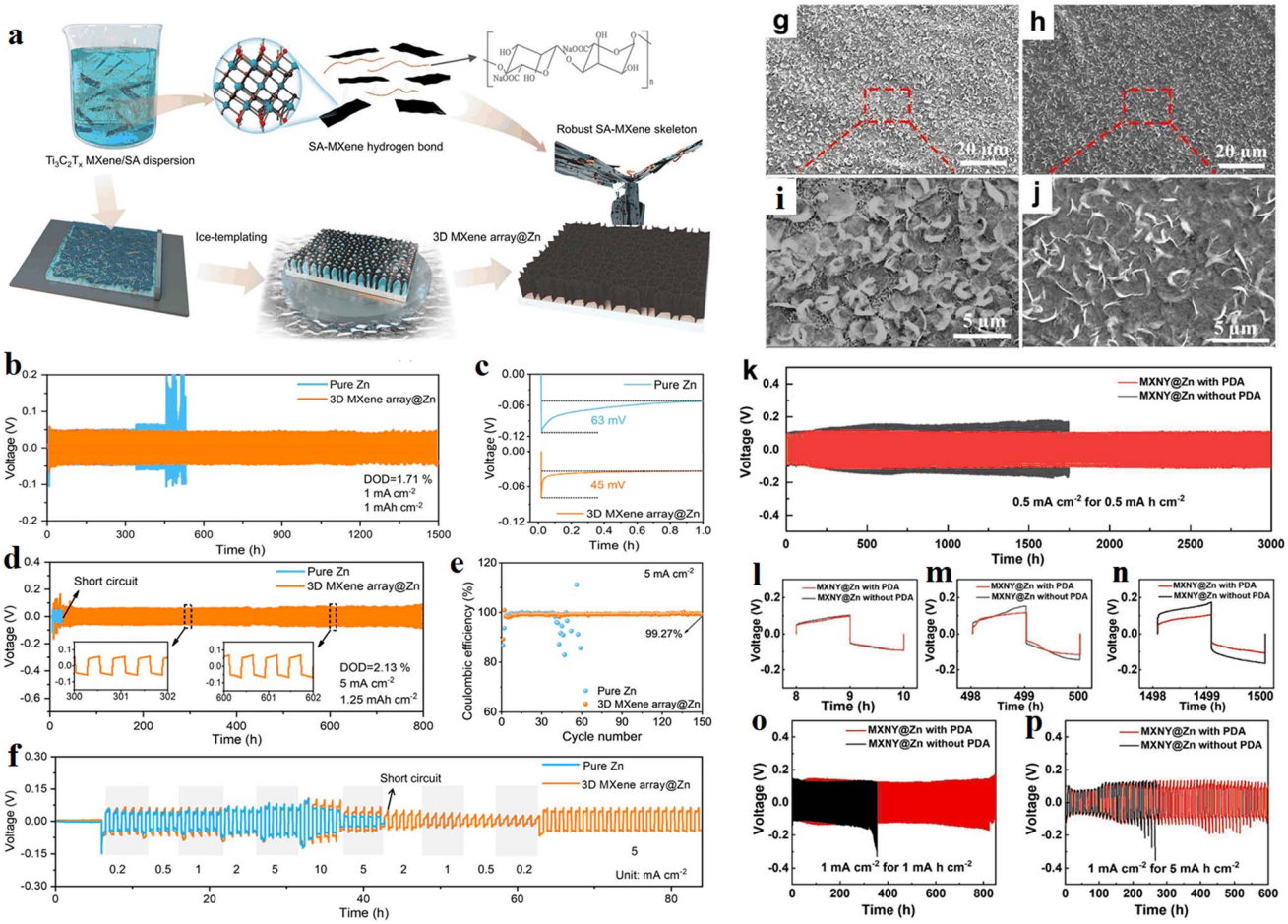

Fig. 14 (a) Schematic illustration of the fabrication process of 3D MXene array@Zn. (b) Long-term cycling performance of Zn symmetric cell, and (c) corresponding nucleation overpotential. (d) Long-term cycling performance of Zn symmetric cell. (e) Rate performance test. (f) Coulombic efficiency of Zn/Cu asymmetric cells with 3D MXene array@Zn anode and pure Zn anode. Reproduced with permission from ref. 89. Copyright 2023, The Author(s). (g–j) The morphology of Zn deposition on HLMX, without (g and i) and with (h and j) DA additive. (k) Cycling stability of symmetric MXNY@Zn cells with (red) and without (black) PDA SEI. (l–n) Enlarged voltage profiles. (o and p) Cycling stability. Reproduced with permission from ref. 90. Copyright 2024, The Authors.

5. Summary and outlook

The above research status shows that researchers have used various means to apply MXene and its derivatives to rechargeable Zn-based energy storage devices, achieving uniform deposition and high reversibility of Zn, effectively suppressing the growth of Zn dendrites and enhancing the device performance, which has become a frontier and hot spot in this field. The performance of MXene materials is largely dependent on their surface structure, mainly on their surface functional groups, such as their types and distribution. However, there are still unresolved scientific questions in this field: how do the functional groups of MXene materials guide the highly reversible and uniform deposition of zinc? The mechanism of MXene's effect on the inhibition of zinc dendrite growth is still unclear. This will seriously affect the large-scale application of MXene as a class of advanced materials in zinc metal energy storage devices, and will also affect the further promotion of MXene in other metal energy storage devices. To solve this scientific problem, we need to explore: (1) the influence of MXene materials' functional groups and defect evolution on zinc diffusion/deposition behavior and electrochemical properties. For example, the –OH functional group will evolve into –O functional group at high temperature. Unlike the surfaces of other 2D materials, the end-group functional groups of MXene can be modified or substituted.[92,93] By modulating the functional groups on the MXene surface, novel functional groups such as halogen, amino and sulfur groups can be generated. MXene with different types, distributions and contents of functional groups have significant differences in regulating zinc diffusion and deposition behaviors, and their action patterns and mechanisms need to be investigated in depth. Based on the feature that *in situ* electrochemistry can visually probe the intermediate reaction products and processes, this project proposes to use techniques such as *in situ* electrochemical infrared spectroscopy and *in situ* Raman spectroscopy to deeply investigate the evolutionary information of MXene's functional groups (chemical bonds) in zinc diffusion and deposition processes and their effects. In addition to surface functional groups, defects also affect the properties of MXene materials.

Sang *et al.* found a large number of defects on the surface of MXene exfoliated by HF etchant by scanning transmission electron microscopy (STEM), and density flooding theory calculations demonstrated that these defects affect the nearby functional groups and the electron distribution of the material, and surface electrons tend to accumulate in these defect regions, forming local electric field distribution, which will affect the diffusion flux of Zn ions and the active sites for deposition. Therefore, the location and concentration of local defects directly affect the deposition/diffusion path of zinc, and the defects also evolve with the continuous deposition of zinc, but the effect of defects in MXene on the diffusion/deposition behavior of zinc is not known. Based on the characteristics of positron sensitivity to defects, this project will use positron annihilation technique to probe *in situ* the MXene defect types, evolution characteristics and their effects on zinc diffusion and deposition behaviors and electrochemical properties. (2) Information on the formation and evolution of SEI at the electrode/electrolyte interface under the action of MXene. The morphology and structure of the SEI film generated at the surface of the artificial protective layer MXene or at the electrode/electrolyte interface due to zinc deposition under a long time cycle evolve continuously, but the evolutionary information is not clear, which will affect the knowledge and understanding of the laws and mechanisms of MXene inhibition of metal dendrite growth and the development and application of MXene-based rational metal electrode interface design.

The layered two-dimensional material MXene has great promise for applications in supercapacitors, batteries, and electrocatalysis due to its large layer spacing, excellent electrical conductivity, good chemical stability, good hydrophilicity, and adjustable layer spacing. In this review, the research progress of inhibiting metallic lithium, sodium, potassium and zinc dendrites is mainly presented. However, MXene materials still face many problems in the process of inhibiting the growth of metal anode dendrites. (1) MXene materials have the disadvantages of high cost and easy oxidation; (2) although MXene materials can effectively inhibit the growth of metal anode dendrites, the scheme is tedious, and a simple and feasible scheme is still to be found; (3) the mechanism of MXene materials to inhibit metal anode dendrites has not been accurately derived, *etc.*

At present, the research on alkali metal battery/capacitor and zinc metal battery/capacitor is still in the initial stage, and many challenges need to be faced. One of the biggest challenges is the problem of interfacial side reactions and dendrite growth of metal anodes. The interfacial stability of metal anodes directly affects the cycle life and Coulomb efficiency of batteries; therefore, the construction of a stable metal anode interface is of vital importance for the development and design of new high energy density batteries/capacitors. Although some progress has been made at this stage of research on batteries/capacitors, the research on metal anodes still lacks systematic and more reliable theoretical support due to the difficulty of metal anode storage preparation, and there are many shortcomings in its modification work, which requires researchers to combine modern analytical and testing techniques and surface interface engineering for systematic development and design.

Data availability

The authors confirm that the data supporting the findings of this study are available within the article.

Author contributions

Haiyan Wang: writing the first draft, funding acquisition, project administration; Mengxin Ning: investigation, data curation, methodology; Min Sun: formal analysis; Bin Li: formal analysis; Yachuan Liang, formal analysis; Zijiong Li: writing-review & edit.

Conflicts of interest

No conflict of interest exists.

Acknowledgements

This work is supported by Key Research and Promotion Projects in Henan Province (232102231033), as well as Maker Space project in Zhengzhou University of Light Industry (grant number 2021ZCKJ220).

References

1 X. B. Cheng, R. Zhang, C. Z. Zhao, *et al.*, Toward safe lithium metal anode in rechargeable batteries: a review, *Chem. Rev.*, 2017, **117**(15), 10403–10473.
2 B. J. Goodenough, Energy storage materials: a perspective, *Energy Storage Mater.*, 2015, **1**, 158–161.
3 T. Famprikis, P. Canepa, J. A. Dawson, *et al.*, Fundamentals of Inorganic Solid-State Electrolytes for Batteries, *Nat. Mater.*, 2019, **18**(12), 1278–1291.
4 M. R. Palacin and A. De Guibert, Why do Batteries Fail?, *Science*, 2016, **351**(6273), 1253292.
5 N. Zhang, X. Chen, M. Yu, *et al.*, Materials Chemistry for Rechargeable Zinc-Ion Batteries, *Chem. Soc. Rev.*, 2020, **49**(13), 4203–4219.
6 J. M. Tarascon and M. Armand, Issues and Challenges Facing Rechargeable Lithium Batteries, *Nature*, 2001, **414**(6861), 359–367.
7 J. W. Choi and D. Aurbach, Promise and Reality of Post-Lithium-Ion Batteries with High Energy Densities, *Nat. Rev. Mater.*, 2016, **1**(4), 16013.
8 P. P. Lopes and V. R. Stamenkovic, Past, Present, and Future of Lead-Acid Batteries, *Science*, 2020, **369**(6506), 923–924.
9 P. He, T. Zhang, J. Jiang, *et al.*, Lithium-Air Batteries with Hybrid Electrolytes, *J. Phys. Chem. Lett.*, 2016, **7**(7), 1267–1280.
10 E. C. Evarts, Lithium batteries: To the Limits of Lithium, *Nature*, 2015, **526**(7575), S93–S95.

11 Y. Cao, M. Li, J. Lu, *et al.*, Bridging the Academic and Industrial Metrics for Next-Generation Practical Batteries, *Nat. Nanotechnol.*, 2019, **14**(3), 200–207.
12 Q. Zhao, S. Stalin, C. Z. Zhao, *et al.*, Designing Solid-State Electrolytes for Safe, Energy-Dense Batteries, *Nat. Rev. Mater.*, 2020, **5**(3), 229–252.
13 S. Liu, J. Feng, X. Bian, *et al.*, The Morphology-Controlled Synthesis of a Nanoporous-Antimony Anode for High-Performance Sodium-Ion Batteries, *Energy Environ. Sci.*, 2016, **9**(4), 1229–1236.
14 N. Nitta, F. Wu, J. T. Lee, *et al.*, Li-Ion Battery Materials: Present and Future, *Mater. Today*, 2015, **18**(5), 252–264.
15 T. Yuan, *Preparation and Performance Study of MXene Based High Energy Density Secondary Battery Materials*, Shandong University, 2021.
16 B. Chen, S. Sui, F. He, *et al.*, Interfacial engineering of transition metal dichalcogenide/carbon heterostructures for electrochemical energy applications, *Chem. Soc. Rev.*, 2023, **52**(22), 7802–7847.
17 B. Chen, X. Zhong, G. Zhou, *et al.*, Graphene-Supported Atomically Dispersed Metals as Bifunctional Catalysts for Next-Generation Batteries Based on Conversion Reactions, *Adv. Mater.*, 2022, **34**(5), 2105812.
18 Y. Wang, Y. Cheng, B. Chen, *et al.*, p-band regulation guides the free-standing porous carbon electrode for efficient Na-CO_2 batteries, *Energy Storage Mater.*, 2024, **71**, 103655.
19 S. Sui, H. Xie, B. Chen, *et al.*, Highly Reversible Sodium-ion Storage in A Bifunctional Nanoreactor Based on Single-atom Mn Supported on N-doped Carbon over MoS_2 Nanosheets, *Angew. Chem., Int. Ed.*, 2024, **63**(27), e202401238.
20 B. Chen, Z. Qi, B. Chen, *et al.*, Room-Temperature Salt Template Synthesis of Nitrogen-Doped 3D Porous Carbon for Fast Metal-Ion Storage, *Angew. Chem., Int. Ed.*, 2024, **63**(1), e202316116.
21 M. Liang, Ha. Zhang, B. Chen, *et al.*, A Universal Cross-Synthetic Strategy for Sub-10 nm Metal-Based Composites with Excellent Ion Storage Kinetics, *Adv. Mater.*, 2023, **35**, 2307209.
22 M. R. Lukatskaya, S. Kota, Z. F. Lin, *et al.*, Ultra-high-rate pseudocapacitive energy storage in two-dimensional transition metal carbides, *Nat. Energy*, 2017, **2**(8), 171051111.
23 M. Ghidiu, M. R. Lukatskaya, M. Q. Zhao, *et al.*, Conductive two-dimensional titanium carbide 'clay' with high volumetric capacitance, *Nature*, 2014, **516**(7529), 78–81.
24 M. Naguib, V. N. Mochalin, M. W. Barsoum, *et al.*, 25th anniversary article: MXenes: a new family of two-dimensional materials, *Adv. Mater.*, 2014, **26**(7), 992–1005.
25 X. Wang, Preparation and Electrochemical Performance of MXene Based Supercapacitor Electrode Materials, PhD thesis, University of Science and Technology of China, 2020, DOI: **10.27517/d.cnki.gzkju.2020.001195**, **https://cdmd.cnki.com.cn/Article/CDMD-10358-1020092542.htm**.
26 M. Naguib, M. Kurtoglu, V. Presser, *et al.*, Two-dimensional nanocrystals produced by exfoliation of Ti_3AlC_2, *Adv. Mater.*, 2011, **23**(37), 4248–4253.
27 M. Naguib and Y. Gogotsi, Synthesis of two-dimensional materials by selective extraction, *Acc. Chem. Res.*, 2015, **48**(1), 128–135.
28 M. Naguib, O. Mashtalir, J. Carle, *et al.*, Two-dimensional transition metal carbides, *ACS Nano*, 2012, **6**(2), 1322–1331.
29 M. Ghidiu, M. Naguib, C. Shi, *et al.*, Synthesis and characterization of two-dimensional Nb_4C_3 (MXene), *Chem. Commun.*, 2014, **50**(67), 9517–9520.
30 M. Naguib, J. Halim, J. Lu, *et al.*, New two-dimensional niobium and vanadium carbides as promising materials for li-ion batteries, *J. Am. Chem. Soc.*, 2013, **135**(43), 15966–15969.
31 M. Kurtoglu, M. Naguib, Y. Gogotsi, *et al.*, First principles study of two-dimensional early transition metal carbides, *MRS Commun.*, 2012, **2**(4), 133–137.
32 B. Anasori, Y. Xie, M. Beidaghi, *et al.*, Two dimensional, ordered, double transition metals carbides (MXenes), *ACS Nano*, 2015, **9**(10), 9507–9516.
33 T. L. Tan, H. M. Jin, M. B. Sullivan, *et al.*, High-throughput survey of ordering configurations in MXene alloys across compositions and temperatures, *ACS Nano*, 2017, **11**(5), 4407–4418.
34 Y. Xie, Y. DalAgnese, M. Naguib, *et al.*, Prediction and characterization of MXene nanosheet anodes for non-lithium-ion batteries, *ACS Nano*, 2014, **8**(9), 9606–9615.
35 J. Pang, R. G. Mendes, A. Bachmatiuk, *et al.*, Applications of 2D MXenes in energy conversion and storage systems, *Chem. Soc. Rev.*, 2019, **48**(1), 72–133.
36 M. Naguib, J. Come, B. Dyatkin, *et al.*, MXene: a promising transition metal carbide anode for lithium-ion batteries, *Electrochem. Commun.*, 2012, **16**(1), 61–64.
37 J. Come, M. Naguib, P. Rozier, *et al.*, A non-aqueous asymmetric cell with a Ti_2C-based two-dimensional negative electrode, *J. Electrochem. Soc.*, 2012, **159**(8), A1368–A1373.
38 H. Qu, Y. Wang, Y. S. Ye, *et al.*, A promising nanohybrid of silicon carbide nanowires scrolled by graphene oxide sheets with a synergistic effect for poly (propylene carbonate) nanocomposites, *J. Mater. Chem. A*, 2017, **5**(42), 22361–22371.
39 L. Wang, P. Yang, Y. Liu, *et al.*, Scrolling up graphene oxide nanosheets assisted by self-assembled monolayers of alkanethiols, *Nanoscale*, 2017, **9**(28), 9997–10001.
40 X. Chen, R. A. Boulos, J. F. Dobson, *et al.*, Shear induced formation of carbon and boron nitride nano-scrolls, *Nanoscale*, 2013, **5**(2), 498502.
41 F. Wang, X. Wu, X. Yuan, *et al.*, Latest advances in supercapacitors: from new electrode materials to novel device designs, *Chem. Soc. Rev.*, 2017, **46**(22), 6816–6854.
42 S. Q. Shen, Q. Wu and J. Li, Current status of research on the preparation, electrochemical energy storage properties of MXene materials, *J. Mater. Sci. Eng.*, 2021, **39**(3), 515–526.
43 L. Niu, P. Wang, L. Zhang, *et al.*, Research progress on the preparation of $Ti_3C_2T_x$ MXene and its application in supercapacitors, *J. Synth. Cryst.*, 2021, **50**(11), 2183–2191.
44 Q. Man, Y. An, H. Shen and J. Feng, MXenes and Their Derivatives for Advanced Solid-State Energy Storage Devices, *Adv. Funct. Mater.*, 2023, **33**, 2303668.
45 Y. An, Y. Tian, H. Shen and J. Feng, Two-dimensional MXenes for flexible energy storage devices, *Energy Environ. Sci.*, 2023, **16**, 4191.

46 Z. Wang, C. Wei, H. Jiang and J. Feng, MXene-Based Current Collectors for Advanced Rechargeable Batteries, *Adv. Mater.*, 2024, **36**(2), 2306015.
47 M. Winter, B. Barnett and K. Xu, Before Li Ion Batteries, *Chem. Rev.*, 2018, **118**(23), 11433–11456.
48 W. Cai, Y. X. Yao, G. L. Zhu, *et al.*, A Review on Energy Chemistry of Fast-Charging Anode, *Chem. Soc. Rev.*, 2020, **49**(12), 3806–3833.
49 X. Chen, X. R. Chen, T. Z. Hou, *et al.*, Lithiophilicity Chemistry of Heteroatom-Doped Carbon to Guide Uniform Lithium Nucleation in Lithium Metal Anodes, *Sci. Adv.*, 2019, **5**(2), eaau7728.
50 D. Lin, J. Zhao, J. Sun, *et al.*, Three-Dimensional Stable Lithium Metal Anode with Nanoscale Lithium Islands Embedded In Ionically Conductive Solid Matrix, *Proc. Natl. Acad. Sci. U. S. A.*, 2017, **114**(18), 4613–4618.
51 A. Pei, G. Zheng, F. Shi, *et al.*, Nanoscale Nucleation and Growth of Electrodeposited Lithium Metal, *Nano Lett.*, 2017, **17**(2), 1132–1139.
52 J. G. Zhang, W. Xu, J. Xiao, *et al.*, Lithium Metal Anodes with Nonaqueous Electrolytes, *Chem. Rev.*, 2020, **120**(24), 13312–13348.
53 C. P. Yang, Y. X. Yin, S. F. Zhang, *et al.*, Accommodating Lithium into 3D Current Collectors with a Submicron Skeleton towards Long-Life Lithium Metal Anodes, *Nat. Commun.*, 2015, **6**, 8058.
54 K. Yan, Z. Lu, H. W. Lee, *et al.*, Selective Deposition and Stable Encapsulation of Lithium through Heterogeneous Seeded Growth, *Nat. Energy*, 2016, **1**(3), 16010.
55 G. X. Li, Z. Liu, Q. Q. Huang, *et al.*, Stable Metal Battery Anodes Enabled by Polyethylenimine Sponge Hosts by Way of Electrokinetic Effects, *Nat. Energy*, 2018, **3**(12), 1076–1083.
56 X. B. Cheng, R. Zhang, C. Z. Zhao, *et al.*, Toward Safe Lithium Metal Anode in Rechargeable Batteries: A Review, *Chem. Soc. Rev.*, 2017, **117**(15), 10403–10473.
57 B. Liu, J. G. Zhang and W. Xu, Advancing Lithium Metal Batteries, *Joule*, 2018, **2**(5), 833–845.
58 Y. Zhang, T. T. Zuo, J. Popovic, *et al.*, Towards better Li metal anodes: Challenges and strategies, *Mater. Today*, 2020, **33**, 56–74.
59 H. Shi, M. Yue, C. J. Zhang, *et al.*, 3D flexible, conductive, and recyclable $Ti_3C_2T_x$ MXene-melamine foam for high-areal-capacity and long-lifetime alkali-metal anode, *ACS Nano*, 2020, **14**(7), 8678–8688.
60 H. Wei, J. Dong, X. Fang, *et al.*, $Ti_3C_2T_x$ MXene/polyaniline (PANI) sandwich intercalation structure composites constructed for microwave absorption, *Compos. Sci. Technol.*, 2019, **169**, 52–59.
61 D. Yang, C. Zhao, R. Lian, *et al.*, Mechanisms of the planar growth of lithium metal enabled by the 2D lattice confinement from a $Ti_3C_2T_x$ MXene intermediate layer, *Adv. Funct. Mater.*, 2021, **31**(24), 2010987.
62 B. Li, D. Zhang, Y. Liu, *et al.*, Flexible Ti_3C_2 MXene-lithium film with lamellar structure for ultrastable metallic lithium anodes, *Nano Energy*, 2017, **39**, 654–661.
63 X. Chen, M. Shang and J. Niu, Inter-layer-calated thin Li metal electrode with improved battery capacity retention and dendrite suppression, *Nano Lett.*, 2020, **20**(4), 2639–2646.
64 Y. Wang, W. Zhang, X. Zeng, *et al.*, Membranes for Separation of Alkali/Alkaline Earth Metal Ions: A Review, *Sep. Purif. Technol.*, 2021, **278**(10), 119640.
65 Y. Fang, Y. Zhang, K. Zhu, *et al.*, Lithiophilic three-dimensional porous $Ti_3C_2T_x$-rGO membrane as a stable scaffold for safe alkali metal (Li or Na) anodes, *ACS Nano*, 2019, **13**(12), 14319–14328.
66 Y. H. Liu, C. Y. Wang, S. L. Yang, *et al.*, 3D MXene architectures as sulfur hosts for high-performance lithium-sulfur batteries, *J. Energy Chem.*, 2022, **66**, 429–439.
67 H. Shi, C. J. Zhang, P. Lu, *et al.*, Conducting and lithiophilic MXene/graphene framework for high-capacity, dendrite-free lithium-metal anodes, *ACS Nano*, 2019, **13**(12), 14308–14318.
68 L. Li, Y. Zheng, J. Xu, *et al.*, Structural and Interfacial Engineering Strategies for Constructing Dendrite-Free Zinc Metal Anodes, *ACS Energy Lett.*, 2024, **9**(7), 3269–3289.
69 H. Liu, Z. Xin, B. Cao, *et al.*, Versatile MXenes for Aqueous Zinc Batteries, *Adv. Sci.*, 2024, **11**, 2305806.
70 T. Bashir, S. Zhou, S. Yang, *et al.*, Progress in 3D-MXene Electrodes for Lithium/Sodium/Potassium/Magnesium/Zinc/Aluminum-Ion Batteries, *Electrochem. Energy Rev.*, 2023, **6**, 5.
71 S. Bai, Z. Huang, G. Liang, *et al.*, Electrolyte Additives for Stable Zn Anodes, *Adv. Sci.*, 2024, **11**, 2304549.
72 N. Zhang, S. Huang, Z. Yuan, *et al.*, Direct self-assembly of MXene on Zn anodes for dendrite-free aqueous zinc-ion batteries, *Angew. Chem., Int. Ed.*, 2021, **60**(6), 2861–2865.
73 X. Li, M. Li, K. Luo, *et al.*, Lattice Matching and Halogen Regulation for Synergistically Induced Uniform Zinc Electrodeposition by Halogenated Ti_3C_2 MXenes, *ACS Nano*, 2022, **16**(1), 813–822.
74 Y. Li, Q. Zhu, M. Xu, *et al.*, Cu-Modified $Ti3C_2Cl_2$ MXene with Zincophilic and Hydrophobic Characteristics as a Protective Coating for Highly Stable Zn Anode, *Adv. Funct. Mater.*, 2023, **33**, 2213416.
75 G. Zhu, H. Zhang, J. Lu, *et al.*, 3D Printing of MXene-Enhanced Ferroelectric Polymer for Ultrastable Zinc Anodes, *Adv. Funct. Mater.*, 2024, **34**, 2305550.
76 J. Gao, X. Zhang, M. Wang, *et al.*, Uniform Zinc Deposition Regulated by a Nitrogen-Doped MXene Artificial Solid Electrolyte Interlayer, *Small*, 2023, **19**, 2300633.
77 Y. Li, Z. Pang, A. Ghani, *et al.*, Gradient Structural and Compositional Design of Conductive MXene Aerogels for Stable Zn Metal Anodes, *Adv. Energy Mater.*, 2023, **13**, 2301557.
78 T. Wang, K. Yao, K. Li, *et al.*, Influence of MXene-assisted multifunctional interface on zinc deposition toward highly reversible dendrite-free zinc anodes, *Energy Storage Mater.*, 2023, **62**, 102921.
79 Y. Wang, T. Ren, Z. Wang, *et al.*, Enabling and Boosting Preferential Epitaxial Zinc Growth *via* Multi-Interface Regulation for Stable and Dendrite-Free Zinc Metal Batteries, *Adv. Energy Mater.*, 2024, **14**, 2400613.
80 X. Liu, Y. Fang, P. Liang, *et al.*, Surface-tuned two-dimension MXene scaffold for highly reversible zinc metal anode, *Chin. Chem. Lett.*, 2021, **32**(9), 2899–2903.

81 C. Sun, C. Wu, X. Gu, *et al.*, Interface engineering *via* $Ti_3C_2T_x$ MXene electrolyte additive toward dendrite-free zinc deposition, *Nano-Micro Lett.*, 2021, **13**, 1–13.
82 Z. Chen, X. Li, D. Wang, *et al.*, Grafted MXene/polymer electrolyte for high performance solid zinc batteries with enhanced shelf life at low/high temperatures, *Energy Environ. Sci.*, 2021, **14**(6), 3492–3501.
83 D. R. Kumar, R. Karthik, M. Hasan, *et al.*, Mo-MXene-filled gel polymer electrolyte for high-performance quasi-solid-state zinc metal batteries, *Chem. Eng. J.*, 2023, **473**, 145207.
84 C. Liu, Y. Tian, Y. An, *et al.*, Robust and flexible polymer/MXene-derived two dimensional TiO_2 hybrid gel electrolyte for dendrite-free solid-state zinc-ion batteries, *Chem. Eng. J.*, 2022, **430**, 132748.
85 Y. An, Y. Tian, C. Liu, *et al.*, Rational Design of Sulfur-Doped Three-Dimensional $Ti_3C_2T_x$ MXene/ZnS Heterostructure as Multifunctional Protective Layer for Dendrite-Free Zinc-Ion Batteries, *ACS Nano*, 2021, **15**(9), 15259–15273.
86 J. Zhou, M. Xie, F. Wu, *et al.*, Encapsulation of Metallic Zn in a Hybrid MXene/Graphene Aerogel as a Stable Zn Anode for Foldable Zn-Ion Batteries, *Adv. Mater.*, 2022, **34**(1), 2106897.
87 Z. Fan, J. Jin, C. Li, *et al.*, 3D-printed Zn-ion hybrid capacitor enabled by universal divalent cation-gelated additive-free Ti_3C_2 MXene ink, *ACS Nano*, 2021, **15**(2), 3098–3107.
88 Z. Li, D. Guo, D. Wang, *et al.*, Exploration of Metal/Ti_3C_2 MXene-derived composites as anode for high-performance zinc-ion supercapacitor, *J. Power Sources*, 2021, **506**, 230197.
89 J. Ruan, D. Ma, K. Ouyang, *et al.*, 3D Artificial Array Interface Engineering Enabling Dendrite-Free Stable Zn Metal Anode, *Nano-Micro Lett.*, 2023, **15**, 37.
90 Z. Wang, P. Zhang, J. Zhang, *et al.*, Dendrite-free zinc deposition enabled by MXene/nylon scaffold and polydopamine solid-electrolyte interphase for flexible zinc-ion batteries, *Energy Storage Mater.*, 2024, **67**, 103298.
91 X. Wang, Y. Wang, Y. Jiang, *et al.*, Tailoring ultrahigh energy density and stable dendrite-free flexible anode with $Ti_3C_2T_x$ MXene nanosheets and hydrated ammonium vanadate nanobelts for aqueous rocking-chair zinc ion batteries, *Adv. Funct. Mater.*, 2021, **31**(35), 2103210.
92 V. Kamysbayev, A. S. Filatov, H. Hu, *et al.*, Covalent surface modifications and superconductivity of two-dimensional metal carbide MXenes, *Science*, 2020, **369**(6506), 979–983.
93 Y. Li, H. Shao, Z. Lin, *et al.*, A general Lewis acidic etching route for preparing MXenes with enhanced electrochemical performance in non-aqueous electrolyte, *Nat. Mater.*, 2020, **19**(8), 894–899.